Missing SO$_2$ Oxidant in the Coastal Atmosphere? –

Observations from High Resolution Measurements of OH and Atmospheric

Sulfur Compounds

H. Berresheim, M. Adam, C. Monahan, C. O'Dowd,

School of Physics & Centre for Climate and Air Pollution Studies,

National University of Ireland Galway, Ireland

J.M.C. Plane,

School of Chemistry, University of Leeds, United Kingdom,

B. Bohn, and F. Rohrer*

Institute for Energy and Climate Research (IEK-8), Research Center Jülich, Germany.

*corresponding author

1   **Abstract**

2   Diurnal and seasonal variations of gaseous sulfuric acid (H_2SO_4) and methane

3   sulfonic acid (MSA) were measured in N.E. Atlantic air at the Mace Head

4   atmospheric research station during the years 2010 and 2011. The measurements

5   utilized selected ion / chemical ionization mass spectrometry (SI/CIMS) with a

6   detection limit for both compounds of 4.3×10^4 cm^{-3} at 5 min signal integration. The

7   H_2SO_4 and MSA gas-phase concentrations were analysed in conjunction with the

8   condensational sink for both compounds derived from 3 nm – 10 μm (aerodynamic

9   diameter) aerosol size distributions. Accommodation coefficients of 1.0 for H_2SO_4

10   and 0.12 for MSA were assumed leading to estimated atmospheric lifetimes of the

11   order of 7 min and 25 min, respectively. With the SI/CIMS instrument in OH

12   measurement mode alternating between OH signal and background (non-OH) signal

13   evidence was obtained for the presence of one or more unknown oxidants of SO_2 in

14   addition to OH. Depending on the nature of the oxidant(s) their ambient concentration

15   may be enhanced in the CIMS inlet system by additional production. The apparent

16   unknown SO_2 oxidant was additionally confirmed by direct measurements of SO_2 in

17   conjunction with calculated H_2SO_4 concentrations. The calculated H_2SO_4

18   concentrations were consistently lower than the measured concentrations by a factor

19   4.7 ± 2.4 when considering the oxidation of SO_2 by OH as the only source of H_2SO_4.

20   Both the OH and the background signal were also observed to increase significantly

21   during daytime aerosol nucleation events, independent of the ozone photolysis

22   frequency, $J(O^1D)$, and were followed by peaks in both H_2SO_4 and MSA

23   concentrations. This suggests a strong relation between the unknown oxidant(s), OH

24   chemistry, and the atmospheric photolysis and photo-oxidation of biogenic iodine

25   compounds. As to the identity of the atmospheric SO_2 oxidant(s), we have been able

to exclude ClO, BrO, IO, and OIO as possible candidates based on *ab initio*

calculations. Nevertheless, IO could contribute significantly to the observed CIMS

background signal. A detailed analysis of this CIMS background signal in context

with recently published kinetic data currently suggests that Criegee intermediates

(CI's) produced from ozonolysis of alkenes play no significant role for SO_2 oxidation

in the marine atmosphere at Mace Head. On the other hand, SO_2 oxidation by small

CI's such as CH_2OO produced photolytically or possibly in the photochemical

degradation of methane is consistent with our observations. In addition, H_2SO_4

formation from dimethylsulfide oxidation via SO_3 as intermediate instead of SO_2 also

appears to be a viable explanation. Both pathways need to be further explored.

1. Introduction

It has been well established that homogeneous oxidation of tropospheric gases is

generally dominated by reactions with the hydroxyl (OH) radical during daylight

hours and - in regions with significant nitrogen oxide, NOx, concentrations - with the

nitrate (NO_3) radical in the absence of sunlight [Stone et al., 2012]. Reactions of

molecular oxygen, ozone, or peroxy radicals such as HO_2 and RO_2 (R = organic rest

molecule) are comparatively slow, with few exceptions, such as $NO + HO_2$ which

recycles OH [e.g., Atkinson et al., 2004]. Heterogeneous oxidation (on the surface of

aerosol particles and in cloud and fog droplets) is dominated either by reactions with

dissolved ozone, hydrogen peroxide, or molecular oxygen, the latter pathway being

catalyzed by transition metal ions [Harris et al., 2013; Berresheim and Jaeschke,

1986]. However, recent studies have revived an interest in the formation and fate of

atmospheric Criegee intermediates (radical species produced from reactions of ozone

51   with alkenes [Calvert et al., 2000; Criegee, 1975]) which to this day have eluded

52   direct measurements in the atmosphere since Cox and Penkett [1971] first suggested

53   their potentially important role. Field and laboratory measurements [Berndt et al.,

54   2014; Stone et al., 2014; Taatjes et al., 2014; Berndt et al., 2012; Mauldin et al., 2012;

55   Welz et al., 2012] as well as theoretical and modelling studies [Sarwar et al., 2014;

56   Boy et al., 2013; Vereecken et al., 2012] now suggest that the reactivity of these types

57   of radicals towards compounds such as SO_2 may have been underestimated by at least

58   two orders of magnitude (see also the recent review by Taatjes et al. [2014]).

59   Therefore, in addition to OH - or possibly even rivalling OH chemistry - Criegee

60   intermediates may, under certain conditions, be significant contributors to

61   atmospheric sulfuric acid formation and the production of hygroscopic sulfate

62   particles which can be activated as cloud condensation nuclei (CCN).

63

64   Selected ion – chemical ionization mass spectrometry (SI/CIMS) has been pioneered

65   by Eisele and coworkers [Tanner and Eisele, 1995; Eisele and Tanner, 1993, 1991] for

66   high time resolution measurements of OH, H_2SO_4, MSA(g) (gaseous methane

67   sulfonic acid), and other compounds in the troposphere. A large number of field

68   studies both on the ground as well as airborne have been successfully conducted using

69   this technique and significantly improved our understanding of tropospheric chemistry

70   [e.g., Stone et al., 2012; Huey, 2007; Heard and Pilling, 2003]. In some of these

71   studies it has already been conjectured that SI/CIMS may also provide information

72   about the presence of atmospheric oxidants other than OH by analyzing the

73   background signal recordings obtained in the OH measurement mode. Specifically,

74   the identity of those "background X-oxidant(s)" was speculated to be Criegee

75 intermediates because of their observed reactivity towards SO_2 in the measurement

76 system [e.g., Berresheim et al., 2002].

77

78 In the present paper we have analyzed two years of SI/CIMS measurements made at

79 Mace Head, Ireland, for significant occurrences of such background signals indicating

80 the presence of one or more unknown SO_2 oxidants in coastal air which could

81 contribute to H_2SO_4 formation (in addition to OH) during day- and nighttime.

82 Furthermore, balance calculations of ambient H_2SO_4 levels using measured SO_2, OH,

83 and aerosol particle concentrations have been compared with measured H_2SO_4 levels.

84 This allowed us to approximate corresponding contributions to ambient H_2SO_4 levels

85 from oxidation of SO_2 by oxidants other than OH and estimate their relative

86 importance with respect to OH reactivity.

87

88 **2. Experimental**

89

90 A principle scheme of the Mace Head CIMS instrument and its operation is shown in

91 Figure 1. Similar to previously described systems [Berresheim et al., 2013; 2000;

92 Mauldin et al., 2012; 1998] the aerodynamically shaped main air inlet extrudes

93 retractably through the wall of the building, here towards the open ocean with a

94 marine wind sector of 190°-300°. In the following text, "marine sector" data includes

95 only the subset of data consistent with the marine wind sector, NO levels < 50 pptv,

96 and/or black carbon concentrations < 50 ng m^{-3}. From the main air flow

97 (approximately 2.5 m^3 hr^{-1}) the central region is sampled at 12 slpm through a 1.9 cm

98 diameter sample flow tube. Two pairs of oppositely arranged capillary stainless steel

99 injectors (the front pair sitting upflow, the rear pair downflow at 5.2 cm distance from

each other) protrude into the sample flow tube. Depending on the operational mode

(OH signal measurement, OH background measurement, or H_2SO_4 and MSA(g)

measurement) selected flows of SO_2, propane (C_3H_8), and N_2 (as make-up gas) are

added through the injectors to the sample flow.

For measuring an OH signal isotopically heavy $^{34}SO_2$ (98.8%, Eurisotop, Saint-Aubin,

France) is introduced through the front injectors and mixed into the sample air flow

resulting in a SO_2 mixing ratio of approximately 8 ppmv. At this setting, the OH

lifetime (1/e definition) in the sample flow is 6 ms. The ambient OH concentration

introduced into the CIMS system is completely converted to $H_2^{34}SO_4$ by its reaction

with $^{34}SO_2$ within the available reaction time of $\tau_{reac,OH} = 78$ ms before reaching the

rear injectors. Approximately 1% of the resulting product, $H_2^{34}SO_4$, is converted via

chemical ionization at atmospheric pressure by NO_3^- reactant ions into $H^{34}SO_4^-$

product ions which are then focussed and guided by electrical potentials (along with

remaining NO_3^- ions) through a 80 μm aperture into the vacuum mass spectrometry

region. The reactant ions are produced in a sheath flow of purified ambient air with

added HNO_3 passing by a radioactive ^{241}Am alpha emitter (activity: 4.1 MBq; Eckert

& Ziegler, Berlin, Germany). Detection of the $H^{34}SO_4^-$ signal at m/z 99 following

quadrupole mass filtering yields the equivalent concentration of OH in ambient air.

Applying the same method of ionization, ambient sulfuric acid, H_2SO_4, and methane

sulfonic acid, CH_3SO_3H, in which sulfur occurs as ^{32}S at a fraction of 0.95 [Krouse

and Grinenko, 1991] are detected at m/z 97 and m/z 95, respectively. Time resolution

for measuring all three masses is typically 30 s. In general, measurement signals are

integrated to 5 min with corresponding detection limits of 1.3×10^5 cm^{-3} for OH and

4.3×10^4 cm^{-3} for both H_2SO_4 and MSA(g), respectively [Berresheim et al., 2013;

125   Mauldin et al., 1998]. Further details including calibration procedures can be found in

126   Berresheim et al. [2000]. The operational cycle of the CIMS instrument was typically

127   set to measure ambient OH and H_2SO_4 for 5 min during each half hour, followed by

128   25 min measurements of ambient H_2SO_4 and MSA(g).

129   Propane (99.95%, Air Liquide, UK) is introduced into the sample flow through the

130   rear injectors (establishing a mixing ratio of approximately 430 ppmv in the sample

131   flow) to scavenge any OH which might be recycled from peroxy radicals via reaction

132   with nitric oxide, NO. On average, nighttime OH measurements showed no statistical

133   difference between the background signal and the OH signal suggesting any potential

134   interference by trace contaminants in the propane to be negligible. Due to similar rate

135   constants for SO_2 and propane with respect to their reaction with OH (both ca. 1×10^{-12}

136    $cm^3 \, s^{-1}$ at 298 K; Atkinson et al. [2004]) any (recycled) OH molecules are completely

137   scavenged by propane instead of SO_2 from this point, i.e., downflow from the rear

138   injectors. Due to the very low NO mixing ratios in marine air at Mace Head

139   [Berresheim et al., 2013] contributions to the measurement signal from the recycling

140   of OH are expected to be negligible.

141

142   The background (BG) signal in the OH measurement mode is evaluated by switching

143   the propane flow from the rear to the front injectors. This prevents formation of

144    $H^{34}SO_4^-$ ions resulting from $^{34}SO_2$ + OH reaction in the system. Theoretically, any

145   background counts observed at m/z 99 under these conditions should only reflect the

146   4.2% fraction of ^{34}S occurring in ambient H_2SO_4. If a significantly higher BG count is

147   observed this might indicate the presence of a compound with stronger electron

148   affinity than HNO_3 ending up as a product ion at m/z 99. However, experiments

149   conducted without $^{34}SO_2$ in the system never showed any evidence for the existence

150 of such a compound. Therefore, observations of significant BG signals (above the

151 ambient 4.2% $H^{34}SO_4^-$ signal) suggested the presence of one or more unknown

152 oxidants (X-oxidants) converting $^{34}SO_2$ to $H_2^{34}SO_4$ in the CIMS system without

153 appreciably reacting with propane. Indeed this interpretation was corroborated by

154 stopping the SO_2 injection to the sample flow and observing a corresponding

155 reduction in the m/z 99 BG signal. Furthermore, with SO_2 in the system, the propane

156 flow through the front injector was successively increased from relatively low values

157 up to the operational setting for measuring the BG signal. Before reaching this setting

158 the signal was found to tail off to a background level corresponding to the complete

159 removal of OH. Increasing the propane flow did not further alter the BG signal. Also,

160 no significant BG signal was observed during calibration runs in which OH

161 concentrations on the order of 10^7 -10^8 cm^{-3} were produced from UV photolysis of

162 water vapor in ambient sample air, thus further corroborating the absence of any

163 artefact process contributing to this signal.

164

165 The total reaction time $\tau_{reac,X}$ available to this unknown X-oxidant to react with SO_2

166 in the system forming H_2SO_4 is the time starting when a unit volume of the sample

167 flow passes the position of the first injector pairs until it reaches the end of the

168 atmospheric pressure ionization region, i.e., the 80 μm aperture (see Figure 1). That

169 time in our system corresponds to 0.45 s, or approximately half a second, which is

170 about six times longer than $\tau_{reac,OH}$. Therefore, the relative importance of X in

171 comparison to the atmospheric SO_2 oxidation efficiency of OH may have to be

172 downscaled dependent on the properties of X and its potential formation and/or

173 regeneration during the reaction time. Moreover, the atmospheric importance of X

174 further depends on the $X + SO_2$ rate constant. This will be examined in detail in the

175 following section.

176

177 Photolysis frequencies of ozone, $J(O^1D)$, and of nitrogen dioxide, $J(NO_2)$, were

178 measured since September 2010 on top of a 10 m tower next to the laboratory

179 building. Both were exchanged with recalibrated systems on a semi-annual basis.

180 Details of the measurement principles and performance of the radiometers have been

181 given by Bohn et al. [2008]. SO_2 was measured in May-August 2011 with a Thermo

182 Systems 43i instrument using a heated sample inlet Teflon tubing (40 ℃) to avoid

183 SO_2 losses due to water condensate. Based on a cycle of 30 min signal and 30 min

184 zero measurements (with an added active charcoal filter) we calculated a 2σ detection

185 limit of 25 pptv for one hour time integration.

186

187 **3. Results and Discussion**

188

189 **3.1. Seasonal cycles and atmospheric lifetimes of H_2SO_4 and MSA(g)**

190

191 Figure 2 shows the mean seasonal cycle of the daily maximum H_2SO_4 concentration

192 in the marine sector at Mace Head which typically occurred between 1000-1400 UTC

193 local time, depending on cloud cover. In general, H_2SO_4 showed a clear diel variation

194 closely correlated with the OH concentration (Fig. 3, top). The reason for this

195 correlation was the relatively homogeneous mixing ratio of the major precursor, SO_2,

196 in the marine atmosphere, as shown for a three months period in Figure 4 (top), and

197 the relatively short lifetime of H_2SO_4 caused by uptake onto aerosol surfaces. This so

198 called condensational sink (CS) showed also low variability on most days (Fig. 4,

9

199   bottom). The mean SO_2 mixing ratio in the open ocean sector was 160 ($\pm$ 50) pptv

200   during these summer months. The average atmospheric lifetime of H_2SO_4 with respect

201   to CS was estimated from scanning mobility particle sizer (SMPS) and aerodynamic

202   particle sizer (APS) measurements using the approach of Fuchs and Sutugin [1971]

203   and Pandis and Seinfeld [1998] to be on the order of 7 minutes assuming an

204   accommodation coefficient of 1.0 [Kolb et al., 2010; Hanson, 2005; Boy et al., 2005],

205   a diffusion coefficient for $H_2SO_4(2\ H_2O)$ of 0.075 atm $cm^2\ s^{-1}$ at 75-85% relative

206   humidity [Hanson, 2005], a mean free path of 105 nm for $H_2SO_4(2\ H_2O)$

207   (corresponding to the Fuchs and Sutugin parameterization), and a hygroscopic growth

208   factor of 1.7 (max. 2.0; 90% RH vs. $\leq$40% RH) [Bialek et al., 2012]. The variability

209   of CS shown in Figure 4 was mainly driven by particle counts, not relative humidity

210   which mostly ranged between 75-85%. Overall, we estimate that CS values can be

211   uncertain by at least a factor of two, mainly due to the uncertainties in the count rates

212   of the SMPS and APS instruments and of the hygroscopic growth factor.

213

214   For Mace Head we assume that except perhaps in winter the predominant source for

215   H_2SO_4 in the marine atmosphere is ultimately biogenic [Lin et al., 2012; Seguin et al.,

216   2010], i.e., the emission and oxidation of dimethyl sulfide (DMS) by OH which yields

217   – via further oxidation of intermediate compounds – the gaseous end products H_2SO_4,

218   dimethyl sulfone ($CH_3SO_2CH_3$, $DMSO_2$), and methane sulfonic acid (CH_3SO_3H,

219   MSA) [Berresheim et al., 1995; 1993a]. As described in the previous section, the two

220   acid compounds are detectable by SI/CIMS using the same instrumental setting as for

221   the OH measurement. Corresponding seasonal cycles of aerosol MSA and non-sea

222   salt sulfate, nss-SO_4, have been measured at Mace Head using high-resolution time-

223   of-flight aerosol mass spectrometry (HR-TOF-MS). Both aerosol compounds as well

224   as their concentration ratio show a clear seasonal maximum in summer [Ovadnevaite

225   et al., 2014].

226

227   The mean seasonal cycle of peak MSA(g) mixing ratios recorded during the same

228   daily time slot as for H_2SO_4 and summarized as monthly means is also shown in

229   Figure 2. Similar to H_2SO_4 and the aerosol sulfur compounds, the highest gas phase

230   MSA(g) levels in the marine atmosphere were observed during the summer months

231   which corroborates the biogenic origin of H_2SO_4 measured in this sector. Adopting a

232   sticking coefficient of 0.12 for the aerosol scavenging of MSA(g) [De Bruyn et al.,

233   1994] we obtained an average atmospheric lifetime of approximately half hour (25

234   min) for this compound. As for H_2SO_4 this is somewhat shorter than previously

235   estimated from measurements off the north-western coast of the United States

236   [Berresheim et al., 1993b], however, still within the same order of magnitude.

237   Ammann et al. [2013] have questioned the earlier results obtained by De Bruyn et al.

238   [1994] and Schweitzer et al. [1998] for the MSA(g) accommodation coefficient and

239   suggested preferring a value close to one as reported in the most recent study by

240   Hanson [2005]. However, in our view, adopting a unity value would be in

241   contradiction to common observations of a relatively slower decline of atmospheric

242   MSA(g) levels in comparison to H_2SO_4 in late afternoon and evening hours which has

243   been well documented in previous field studies [e.g., Eisele and Tanner, 1993] and in

244   our present study. Furthermore, as shown already in a previous campaign at Mace

245   Head [Berresheim et al., 2002], ambient MSA(g) levels typically increased with

246   decreasing relative humidity, including at nighttime. Both observations support that

247   the vapor pressure of MSA(g) is significantly higher compared to H_2SO_4 [e.g.,

248   Kreidenweis and Seinfeld, 1988].

249

3.2. H₂SO₄ mass balance and missing SO₂ oxidant in the marine atmosphere

251

From 2 May to 12 August, 2011, an intensive campaign was conducted at Mace Head including measurements of SO_2. The results allowed the calculation of H_2SO_4 concentrations based on its production by SO_2 oxidation by OH and removal due to condensation on existing aerosol surface (CS, condensational sink rate) assuming steady state:

257

$$[H_2SO_4]_{calc} = \frac{k_{OH}[SO_2][OH]}{CS} \tag{1}$$

259

Comparison with measured H_2SO_4 concentrations showed a significant underestimation using eq. (1), bearing in mind the uncertainty in CS can be a factor of two. For the available 38 days with concurrent H_2SO_4, $J(O^1D)$, CS, and SO_2 observations, the mean ratio, i.e., $[H_2SO_4]_{meas}/[H_2SO_4]_{calc}$, was 4.7 ± 2.4 during the midday periods 1000-1400 UTC taking calculated OH values from the relation OH-$J(O^1D)$ (see below). The results for 26 days with direct OH observations out of these 38 are 5.0 ± 2.4 based on the sparse direct OH observations and 4.8 ± 2.5 based on the denser OH values calculated from $J(O^1D)$. All of these results are considerably higher than the mean of 2.4 reported by Mauldin et al. [2012] for a boreal forest site in Finland. An extreme example from 18 June, 2011, is shown in Figure 5a. On average, the measured H_2SO_4 concentrations on this day were a factor of 7 higher than the values calculated by eq. (1) and the background signal shows a strong diel cycle in phase with that of OH. Here we have filled the gaps in our OH measurements by using $J(O^1D)$ as proxy based on the $J(O^1D)$-OH relationship established in Berresheim

12

274 et al. [2013] to obtain calculated H_2SO_4 for each of the measured H_2SO_4 values

275 (continuous red line in top of Fig. 5a). The results demonstrate the close tracking of

276 the measured data and thus, the usefulness of this proxy application. In addition, the

277 open symbols show the corresponding values based on the actual measured (5 min

278 averaged) OH signals from that day (count rates shown in bottom of Fig. 5a) . As can

279 be seen, the latter procedure results in an average discrepancy factor of 5.6 ± 1.2

280 which agrees well with the above factor of 7.0 within given uncertainties.

281

282 Four-day NOAA HYSPLIT air mass back-trajectories for 18 June, 2011,

283 (http://ready.arl.noaa.gov/HYSPLIT.php) in conjunction with MODIS satellite

284 imagery (http://neo.sci.gsfc.nasa.gov) of chlorophyll pigments in surface seawater

285 pointed towards high biogenic sulfur (DMS) contributions to the advected air derived

286 from phytoplankton blooms between Greenland and Iceland. On the other hand, no

287 significant changes were observed in ambient SO_2 levels on the same day. Even

288 higher H_2SO_4 and also MSA(g) concentrations (both in the mid-10^7 cm^{-3} range) were

289 measured on 11 June, 2011, with similar air mass trajectories and SO_2 levels as on 18

290 June, resulting in a measured/calculated H_2SO_4 ratio of 9. A notable difference

291 between both days was the occurrence of low tide at noon on 18 June whereas high

292 tide prevailed at noon on 11 June, respectively.

293

294 A contrasting example is shown in Figure 5b for 10 May, 2011, with a ratio of only

295 1.8 which in view of the overall uncertainties discussed earlier suggests a nearly

296 closed H_2SO_4 balance based on the SO_2 +OH pathway alone. Weather conditions on

297 that day were strongly anticyclonic with no indication of major contributions from

298 biologically active open ocean regions and with overall low solar insolation, i.e., lack

299   of significant photochemistry. The OH background signal did not significantly vary

300   during the day in contrast to the OH concentration itself which despite low insolation

301   still showed a pronounced diel cycle. However, as shown in Figure 6 (e.g., red line),

302   on the vast majority of marine sector days during the 2010 and 2011 measurement

303   periods both the background signal and the OH signal varied in tune with each other

304   which strongly suggests a photolytic source for the unknown compound(s) producing

305   the BG signal.

306

307   Clearly a major source of H_2SO_4 in addition to OH oxidation of SO_2 was missing in

308   the balance calculation based on eq. (1). A similar discrepancy between measured and

309   calculated H_2SO_4 concentrations in the coastal atmosphere of Mace Head was

310   reported previously by Berresheim et al. [2002]. They speculated that the missing

311   source might be DMS oxidation with partial production of SO_3 instead of SO_2 as

312   intermediate, which then readily forms H_2SO_4 with water vapour [Lin and Chameides,

313   1993]. This possibility would also agree with kinetic pathways hypothesized for the

314   DMS + OH oxidation in which CH_3SO_2 and CH_3SO_3 are formed as intermediates,

315   both of which decompose thermally to SO_2 and SO_3, respectively [Berresheim et al.,

316   1995]. Studies at an Antarctic coastal location with strong marine DMS emissions

317   [Jefferson et al., 1998; Davis et al., 1998] reported similar inconsistencies between

318   measured H_2SO_4 levels and SO_2 mixing ratios required to close the mass balance

319   based on SO_2 + OH as the only source, even when assuming a very low H_2SO_4

320   accommodation coefficient of 0.5. Our results shown in Figures 5a and 5b may be

321   consistent with a significant contribution by marine biogenic DMS emissions to

322   H_2SO_4 levels at Mace Head via intermediate production of a precursor other than SO_2.

323   And this influence may even supersede potential regional contributions from

324   emissions which are dependent on tidal cycles as discussed earlier for the cases of 11

325   and 18 June, 2011. However, current uncertainties in our knowledge of DMS

326   oxidation chemistry prevent a quantitative assessment of this potential H_2SO_4 source.

327

328   Alternatively, biogenic emissions of, e.g., organic halogens from the regional coastal

329   environment during low tide may produce highly reactive atmospheric compounds

330   that in addition to OH could play a significant role in atmospheric H_2SO_4 formation.

331   Another class of compounds that have recently been suggested are stabilized Criegee

332   intermediates (sCI) which have been re-evaluated with respect to their potential

333   oxidation of atmospheric SO_2 by Liu et al. [2014], Stone et al. [2014], Welz et al.

334   [2012] and Mauldin et al. [2012]. In the following two sections we investigate the

335   potential importance of SO_2 reactions with some halogen and sCI radicals as sources

336   of H_2SO_4 in addition to the DMS→SO_3 and SO_2 +OH pathways in marine air at Mace

337   Head. The nitrate radical, NO_3, is not expected to be of any importance for nighttime

338   SO_2 oxidation at Mace Head, at least not in air from the marine sector [Berresheim et

339   al., 2013].

340

341   **3.3. Electronic structure calculations on halogen oxide reactions with SO_2**

342

343   Other candidates besides OH acting as SO_2 oxidants might be halogen oxide radicals,

344   however, to our knowledge respective rate constants are available in the literature

345   only for the reactions of IO and ClO with SO_2 [Larin et al., 2000]; DeMore et al.,

346   1997], which are three and six orders of magnitude smaller compared to k_{SO2+OH},

347   respectively. We have made *ab initio* transition state energy calculations for the

348   reactions of SO_2 with ClO, BrO, IO, and OIO using quantum theory. The hybrid

349   density functional / Hartree-Fock B3LYP method was employed from within the

350   Gaussian 09 suite of programs [Frisch et al., 2009], combined with an appropriate

351   basis set for I [Glukhovtsev *et al.*, 1995] and the standard 6-311+g(2d,p) triple zeta

352   basis sets for Br, Cl, O and S. The geometries, rotational constants, vibrational

353   frequencies and relative energies of the transition states are listed in Table 1.

354   Following geometry optimizations of the transition states for the reactions of ClO,

355   BrO, IO and OIO with SO_2, and the determination of their corresponding vibrational

356   frequencies and (harmonic) zero-point energies, energies relative to the reactants were

357   obtained. In the case of BrO and ClO + SO_2, more accurate transition state energies

358   were computed at the CBS-QB3 level [Montgomery et al., 2000]. At this level of

359   theory, the expected uncertainty in the calculated transition state energies should be

360   better than 0.07 eV [Foresman and Frisch, 1996]. Spin-orbit effects were ignored

361   since these are present both in the reactant halogen oxide and the transition state.

362   Figure 7 illustrates the transition state geometries for ClO, BrO, IO and OIO + SO_2.

363

364   Transition state theory (TST) calculations were then carried out using the calculated

365   molecular parameters in Table 1. Although the reaction between IO and SO_2 has a

366   small barrier (7.3 kJ mol^{-1}), the reaction has quite a tight transition state and the TST

367   calculation yields $k(200 - 400 \text{ K}) = 4.3 \times 10^{-14} \exp(-1150/T)$ cm^3 s^{-1}. The resulting

368   value of $k(343 \text{ K}) = 1.6 \times 10^{-15}$ cm^3 s^{-1} is consistent with an experimental upper limit of

369   6×10^{-15} cm^3 s^{-1} determined at that temperature by Larin et al. [1998]. At a marine

370   boundary layer temperature of 293 K, the rate coefficient is only 8.5×10^{-16} cm^3 s^{-1}.

371   This reaction would have to compete with OH + SO_2, which has a rate coefficient of k

372     $= 9 \times 10^{-13}$ cm^3 s^{-1}. Although [IO] can be around 30 times larger than [OH] at midday

373   at Mace Head, the ratio of rate constants is 1/1050, so the OH reaction is about 35

374   times faster. However, the estimated SO_2 + IO rate constant is large enough to allow a

375   fraction of IO to be converted to H_2SO_4 inside the CIMS instrument and to contribute

376   to the background signal (see Section 3.4).

377

378   During nighttime at Mace Head, OIO builds up to a mixing ratio of a few parts per

379   trillion [Saiz-Lopez and Plane, 2004]. However, the very large barrier for the OIO +

380   SO_2 reaction (50.1 kJ mol^{-1}) means that this reaction is negligibly slow: k(200-400 K)

381   = 6.4×10^{-13} exp(-6400/T) cm^3 s^{-1}, and k(293 K) = 2.2×10^{-22} cm^3 s^{-1}.

382

383   BrO has been observed at a mixing ratio of several parts per trillion during the day at

384   Mace Head [Saiz-Lopez et al., 2004]. However, the reaction BrO + SO_2 also has a

385   significant barrier (20.4 kJ mol^{-1}), and so the reaction is much too slow in the MBL:

386   k(200-400 K) = 5.8×10^{-14} exp(-2700/T) cm^3 s^{-1}, and k(293 K) = 5.6×10^{-18} cm^3 s^{-1}.

387   Finally, the TST calculation for ClO + SO_2, which also has a significant barrier (24.1

388   kJ mol^{-1}), yields k = 5.2×10^{-14} exp(-3100/T) cm^3 s^{-1}. The theoretical rate coefficient at

389   298 K is therefore 1.5×10^{-18} cm^3 s^{-1}, which is in accord with an experimental upper

390   limit of 4×10^{-18} cm^3 s^{-1} at this temperature [DeMore et al., 1997]. In summary we

391   conclude that none of the halogen oxides considered here exhibit sufficient turnover

392   rates with SO_2 in ambient air to account for the missing H_2SO_4 source.

393

394

395   **3.4. Could X be a Criegee radical produced from ozonolysis?**

396

397   Previous measurements at Mace Head have shown clear diurnal cycles of light

398   alkenes (including isoprene) with a strong dependence on solar flux [Broadgate et al.,

399   2004; Lewis et al., 1999]. Assuming that "X" is indeed a Criegee intermediate

400   produced from ozonolysis of alkenes and reacting with SO_2 both in the atmosphere

401   and in the CIMS inlet system to produce additional H_2SO_4, we can estimate its

402   relative contribution compared to the SO_2 +OH reaction as follows. (In the following

403   equations, the term sCI is used as a surrogate for sCI (stabilized Criegee

404   intermediates) and CI (Criegee intermediates in general) species.)

405

406   As already pointed out in the Experimental section we have to account for additional

407   formation of $[sCI]_{cims}$ from alkene + O_3 reactions over the total available residence

408   time of 0.45 s in the atmospheric pressure reaction and ionization region of the CIMS

409   instrument (see Fig. 1). By continuous reaction with SO_2 and ionization of the

410   resulting $H_2^{34}SO_4$ molecules over the corresponding distance (32 cm) this leads to an

411   accumulation of the $H^{34}SO_4^-$ background signal at m/z 99 assuming the sCI+SO_2

412   oxidation to be instantaneous at the high SO_2 concentration in the CIMS reactor tube.

413   The enhancement factor EF relative to the ambient air sCI concentration, $[sCI]_{amb}$, is

414    $$EF_{H_2^{34}SO_4} = \frac{[sCI]_{amb} + \int_0^{t_{res}} Prod(sCI) \cdot dt}{[sCI]_{amb}} = 1 + \frac{t_{res}}{\tau_{sCI,amb}} \qquad (2)$$

415   This result is the consequence of the fact that both types of sCI, namely sCI present in

416   ambient air ($[sCI]_{amb} = Prod(sCI) \times \tau_{sCI,amb}$) and sCI produced inside the CIMS inlet are

417   immediately converted to $H_2^{34}SO_4$ by added $^{34}SO_2$ in the CIMS inlet system.

418   Assuming a lifetime with respect to unimolecular decomposition of 0.2 s for sCI

419   compounds resulting from ozonolysis of the monoterpenes α-pinene and limonene

420   [Mauldin et al., supplement, 2012] and the dominant ambient reaction of sCI with

421   water ($k_{H2O+sCI} = 1.4 \times 10^{-17}$ cm^3 s^{-1} (MCM 3.2 http://mcm.leeds.ac.uk/MCM/;

422 Saunders et al. [2003]; Jenkin et al. [2003]), $[H_2O] = 3.1 \times 10^{17}$ cm^{-3} representing Mace

423 Head conditions of T = 14 °C, 75% relative humidity) the ambient lifetime of such

424 stabilized Criegee intermediates is estimated to be 0.1 s. As already mentioned,

425 approximately 1% of the H_2SO_4 is ionized in the CIMS ionization region. Therefore,

426 the production of sCI in this region indeed yields H_2SO_4 via reaction with SO_2, of

427 which, however, only 0.5% is ionized, on average, as this process acts linearly.

428 Consequently, we have to modify eq. (2) to take into account the reduced ionization

429 probability for H_2SO_4 produced in the ionization region:

430

431
$$EF_{H^{34}SO_4^-} = 1 + \frac{t_{reac}}{\tau_{sCI,amb}} + 0.5 \cdot \frac{t_{ion}}{\tau_{sCI,amb}} \qquad (3)$$

432 with t_{res} = 450 ms, t_{reac} = 115 ms, t_{ion} = 335 ms, $\tau^{-1}_{sCI,amb}$ = 1/0.2 s + 4.3 s^{-1} = 9.3 s^{-1}.

433 This formalism is identical to that derived for a similar instrument by Berndt et al.

434 [2012] (chemical ionization time-of-flight mass spectrometer with atmospheric

435 pressure inlet; CI-APi-TOF-MS). Thus, from eq. (3) it follows that $^{34}SO_2$ oxidation by

436 sCI contributes a background signal which represents an enhancement of the ambient

437 sCI concentration by a factor EF = 3.6. Therefore, if X is indeed a sCI compound (of

438 the kind considered here), the measurement signal resulting from sCI would have to

439 be weighted by 1:3.6 with respect to the OH signal to obtain the corresponding

440 ambient air [sCI] concentration.

441

442
$$[sCI]_{amb} = \frac{1}{EF_{H^{34}SO_4^-}} \cdot \frac{BG_{Sig}}{OH_{Sig}} \cdot [OH]_{amb} \qquad (4)$$

443

444 To compare both compounds with respect to their oxidation efficiency towards SO_2,

445 the corresponding rate constants must be factored in as well, i.e., $k_{sCI+SO2}$ / k_{OH+SO2} =

446 6×10^{-13} cm^3 s^{-1}/ 9×10^{-13} cm^3 s^{-1} = 0.67, with k_{OH+SO2} (298 K) = 9×10^{-13} cm^3 s^{-1} taken

447 from Atkinson et al. [2004] and $k_{sCI+SO2}$ adopted for the monoterpene derived sCI +

448 SO_2 reaction as reported by Mauldin et al. [2012].

449

450 This means that the relative oxidation efficiency (ROE) of those ozonolytically

451 generated sCI compounds would be only on the order of 20% compared to that of OH

452 with respect to SO_2 oxidation, assuming that the CIMS background signal is equal to

453 the OH signal as observed on average in the ambient air measurements at Mace Head

454 (see Fig. 6).

455

456
$$\text{ROE} = \frac{k_{sCI+SO_2} \cdot [\text{sCI}]_{\text{amb}} \cdot [\text{SO}_2]_{\text{amb}}}{k_{OH+SO_2} \cdot [\text{OH}]_{\text{amb}} \cdot [\text{SO}_2]_{\text{amb}}}$$
$$= \frac{1}{\text{EF}_{\text{H}^{34}\text{SO}_4^-}} \cdot \frac{\text{BG}_{\text{Sig}}}{\text{OH}_{\text{Sig}}} \cdot \frac{k_{sCI+SO_2}}{k_{OH+SO_2}}$$

(5)

457

458 These calculations depend strongly on the kinetic parameters for the corresponding

459 sCI reactions. In this work we have adopted rate constants published by Mauldin et al.

460 [2012] and Berndt et al. [2012] for relatively large stabilized Criegee intermediates

461 produced from ozonolysis of monoterpenes. However, other studies of smaller

462 Criegee intermediates with low internal energies (CH_2OO by Stone et al. [2014],

463 Berndt et al. [2014], and Welz et al. [2012]; CH_3CHOO by Taatjes et al. [2013])

464 suggest much faster reactions of these CI species with both SO_2 and H_2O,

465 respectively. They are produced from both ozonolysis of alkenes and from photolysis

466 i.e. of CH_2I_2. Furthermore, laboratory studies by Fittschen et al. [2014] and

467 Bossolasco et al. [2014] suggest that CH_2OO could also be produced in the

468 photochemical degradation of methane via the reaction of methyl peroxy radicals

469 CH_3O_2 with OH. For a sensitivity test of the production pathway ozonolysis we

470 neglect the fact, that for the conditions in the CIMS inlet only approximately 80% of

471 these CI would react with the added $^{34}SO_2$. The results are shown in Table 2.

472

473 We find that the oxidation efficiency of sCIs – if formed via ozonolysis - compared to

474 OH would not be significant, based on the condition of equal CIMS background and

475 OH signal counts. The relatively small difference between the estimates for such

476 different species is a consequence of the fact that both reaction parameters (for

477 sCI+SO_2 and sCI+H_2O) are faster for the small Criegee intermediates. The effect of a

478 faster reaction of sCI with SO_2 is almost exactly cancelled out by the faster reactions

479 with H_2O. A special case is CH_2OO for which there is a debate of its reaction rate

480 with water. Berndt et al. [2014] state that CH_2OO reacts fast with H_2O dimers which

481 was not accounted for in previous studies but would dominate the fate of CH_2OO in

482 ambient air at Mace Head. But they could not explain the big difference to the small

483 effects of water vapour on the CH_2OO decay as deduced by Stone at al. [2014] who

484 published a slow reaction constant for CI+H_2O. Anyhow, ROE for CH_2OO for

485 average conditions at Mace Head is calculated to be small taking both sets of

486 parameters from these two publications separately.

487

488 For these reasons, if the oxidant(s) X generating the BG signal of the CIMS

489 instrument would be one of the Criegee intermediates shown in Table 2 and would be

490 produced ozonolytically, the relative oxidation efficiencies for SO_2 by these Criegee

491   intermediates compared to OH for average conditions at Mace Head are estimated to

492   be small, increasing the calculated H_2SO_4 concentration based on the $SO_2 + OH$

493   source alone by only 5-30%. This is still a major shortfall with respect to the average

494   factor of 4.7 required to match the observed ambient air H_2SO_4 concentration.

495

496   On the other hand, if the different Criegee intermediates shown in Table 2 would be

497   produced either photolytically or by reaction of a precursor with OH, the

498   corresponding enhancement factors EF would be 1 (no further production in the

499   CIMS inlet) and the corresponding ROEs would be larger than 10, e.g., for CH_2OO

500   and CH_3CHOO. Taking the CIMS background signal as an upper limit for the

501   estimate of their oxidation efficiency for SO_2 it cannot be excluded that these small

502   Criegee intermediates significantly influence the ambient H_2SO_4 budget at Mace

503   Head. However, given the short atmospheric lifetime of these species we doubt that

504   sufficiently large steady-state concentrations are realistic.

505

506   The consequence for the ambient H_2SO_4 budget at Mace Head is complex. Either 1)

507   very different ozonolytically produced Criegee intermediates than those studied so far,

508   2) photolytically produced Criegee intermediates, 3) Criegee intermediates produced

509   via reactions of OH, 4) an entirely different kind of oxidant for SO_2, or 5) a

510   production process converting a sulfur compound other than SO_2 might be still

511   missing in our present account of the H_2SO_4 concentration in the coastal marine

512   atmosphere.

513

514   Figures 8a and 8b show two out of a few examples of observations we made during

515   the May-August 2011 period which were not obscured by the midday primary OH

516   production period in relation to coastal aerosol nucleation events during which OH

517   and also both H_2SO_4 and MSA(g) concentrations increased significantly in

518   conjunction with a major increase in the background signal counts for the X-

519   oxidant(s). On 13 May, 2011 (Fig. 8a) the first low tide was centered at about 0700

520   UTC. Note that no detectable aerosol nucleation (> 3 nm diameter) occurred at this

521   time as insolation was still low, however, some spikes in both OH concentration and

522   the BG signal were already visible. A significant nucleation event occurred during the

523   second low tide between 1800 and 2100 UTC with somewhat enhanced H_2SO_4 and

524   MSA(g) concentrations. Both the OH concentration and the BG signal again increased

525   as well.

526   On the next day, 14 May, 2011 (Fig. 8b) these effects are even more pronounced with

527   the tide shifted by about +45 min and two major nucleation events clearly detectable.

528   The peak of the morning event at about 0800 UTC coincided with a major production

529   of both OH and the X-compound (BG signal). Conversely to the preceding day, the

530   evening event showed relatively minor OH and X production due to the tidal shift.

531

532   A recent successful H_2SO_4 intercomparison experiment at Mace Head (M. Sipilä and

533   S. Richters, *pers. commun.*, 2013) between the CIMS instrument and a CI-APi-TOF-

534   MS instrument has confirmed that the CIMS indeed measures only the concentration

535   of gaseous "free" (monomeric) H_2SO_4 during nucleation events. With the rapid

536   transition from monomers to multimer clusters in which H_2SO_4 becomes tied up

537   (confined) and not broken down anymore to the HSO_4^- core ions in the CIMS

538   collision dissociation chamber (Fig. 1) a net decrease in ambient H_2SO_4

539   concentrations may therefore be expected. However, as shown in the nucleation

540   events in Figures 8a and 8b, (monomer) H_2SO_4 levels even increased after a certain

23

541 lag time following the onset of the event. We interpret our observations as strong

542 formation of X-oxidant(s) (e.g., CH_2OO from photolysis of CH_2I_2; Welz et al. [2012])

543 or of OH (perhaps via thermal decomposition of sCI; Berndt et al. [2014; 2012], Kroll

544 et al. [2001]) followed by rapid oxidation of DMS and SO_2 to form the products

545 H_2SO_4 and MSA(g). Such coastal nucleation events have previously been shown to be

546 induced by photolysis and photo-oxidation of marine iodine compounds emitted

547 mainly from exposed seaweed during low tide [O'Dowd et al., 2002]. Considering

548 again the $IO+SO_2$ reaction and adopting a rate constant of $k(IO+SO_2) = 8.5 \times 10^{-16}$

549 $cm^3\ s^{-1}$ (section 3.3), we calculate that approximately 8% of atmospheric IO is

550 converting $^{34}SO_2$ to $H_2^{34}SO_4$ in the CIMS inlet system, based on a $^{34}SO_2$ mixing ratio

551 of 8 ppmv and a total IO residence time of 0.45 s. Also, it is assumed that IO does not

552 react with propane. Based on eq. (3) the corresponding yield for $H^{34}SO_4^-$ would be

553 reduced from 8% to 5%. With this estimate an upper limit for the atmospheric IO

554 mixing ratio can be derived from the corresponding CIMS background signal. We

555 estimate ambient IO levels to be, on average, less than 1.3 pptv at noon time (Fig. 6)

556 and less than 5 pptv at the maximum of the nucleation event shown in Figures 8a and

557 8b. This is consistent with previous measurements of IO at Mace Head which showed

558 maximum levels up to 5 pptv [Saiz-Lopez et al., 2006; Alicke et al., 1999]. However,

559 other measurements taken over "hot spots" of exposed seaweed beds have shown IO

560 peak values of up to 50 pptv [Commane et al., 2011]. Thus, it can be concluded that

561 the observed background signal could be explained by the presence of IO that

562 nevertheless would not contribute to atmospheric SO_2 oxidation because of a too

563 small $IO + SO_2$ rate constant. Future studies are required to systematically

564 characterize remaining uncertainties in the CIMS and CS measurements and to verify

565 a possible link between the unknown oxidant(s), the CIMS background, and the

566 iodine cycle in the marine atmosphere.

567

568 **4. Conclusions**

569

570 We observed a persistent but relatively low H_2SO_4 concentration at nighttime (on the

571 order of a few 10^5 cm^{-3}). Also, on some occasions short spikes were observed at

572 nighttime in the H_2SO_4 signal during low tide which might suggest short-term

573 emissions of reactive hydrocarbons capable of forming Criegee intermediates and OH

574 in reactions with ozone which are both capable of oxidizing SO_2. We assume that

575 such processes also happen during daytime but are superimposed by the formation of

576 another major oxidant which shows a similar diurnal pattern like OH. A detailed

577 analysis of the atmospheric H_2SO_4 budget at Mace Head revealed that a dominant

578 oxidant for the production of H_2SO_4 is missing which, on average, would have to

579 contribute 4.7 times more than the observed production from $OH+SO_2$. Whether this

580 oxidant might be a Criegee intermediate with its production mainly determined by

581 strong light-induced emissions of marine alkene species and/or atmospheric

582 photolysis of iodine species remains an open question. However, we consider it

583 unlikely that α-pinene or limonene are present at significant levels in the marine

584 atmosphere. In forest environments these compounds are also emitted at nighttime

585 resulting in a quite different diurnal cycle of the CIMS background signal [Mauldin et

586 al., 2012] than we have observed in the coastal atmosphere. In the present work we

587 have shown that the signal measured with the CIMS instrument during its background

588 mode provides indeed evidence for the presence of one or more unknown oxidants for

589 atmospheric SO_2 in addition to OH. However, as this oxidant X does not significantly

590   react with propane in the CIMS system, the corresponding X-signal must be corrected

591   in some cases to account for additional production inside the CIMS inlet system

592   before evaluating its oxidation efficiency towards SO_2 in ambient air. For this reason

593   and also based on the currently available kinetic data for the SO_2 oxidation by sCI

594   compounds resulting from monoterpenes or from smaller alkenes we conclude that at

595   least Criegee intermediates produced via ozonolysis are unimportant in comparison

596   with the SO_2+OH oxidation in the marine atmosphere at Mace Head. It appears that

597   Mauldin et al. [2012] have not considered this correction which reduces the proposed

598   oxidation efficiency for SO_2 of stabilized Criegee intermediates from ozonolysis of α-

599   pinene or limonene in forested environments as well. Also, our observations do not fit

600   with diel cycles expected to arise from oxidation of SO_2 by ClO, BrO, IO or OIO

601   halogen radicals. On the other hand, CH_2OO formed via photolysis of CH_2I_2 appears

602   to be a candidate to explain the observed increase in the CIMS background signal

603   especially during daytime aerosol nucleation events at low tide, and to have a

604   significant impact on the ambient H_2SO_4 budget. In any case, more comprehensive

605   measurements including alkenes, isoprene, and halogen compounds are needed in

606   conjunction with laboratory kinetic studies to confirm the presence of oxidant species

607   other than OH with significant contributions to the H_2SO_4 budget in the marine

608   atmosphere. An additional source of H_2SO_4 not accounted for by the SO_2 + (OH or X)

609   pathway may be the formation of SO_3 (instead of SO_2) as an intermediate in the

610   oxidation of DMS followed by rapid reaction with water vapour. To better evaluate

611   the contribution from this potential source further studies involving additional

612   measurements of DMS are planned for future work in conjunction with what we have

613   already attempted in the present study, i.e., analysis of air mass advection from

614   biologically active oceanic regions using satellite remote sensing data.

615

625

626

627

628

629

630

631 **References**

632

633 Alicke, B., K. Hebestreit, J. Stutz, and U. Platt, Iodine oxide in the marine boundary

634 layer, *Nature, 397,* 572-573 (1999).

635

636 Ammann, M., R. A. Cox, J. N. Crowley, M. E. Jenkin, A. Mellouki, M. J. Rossi, J.

637 Troe, and T. J. Wallington, Evaluated kinetic and photochemical data for atmospheric

638 chemistry: Volume VI – heterogeneous reactions with liquid substrates, *Atmos. Chem.*

639 *Phys., 13*, 8045–8228 (2013).

640

641 Atkinson, R., D. L. Baulch, R. A. Cox, J. N. Crowley, R. F. Hampson, R. G. Hynes,

642 M. E. Jenkin, M. J. Rossi, and J. Troe, Evaluated kinetic and photochemical data for

643 atmospheric chemistry: Volume I – gas phase reactions of Ox, HOx, NOx and SOx

644 species, *Atmos. Chem. Phys., 4*, 1461−1738 (2004).

645

646 Berndt, T., T. Jokinen, M. Sipilä, R.L. Mauldin III, H. Herrmann, F. Stratmann, H.

647 Junninen, and M. Kulmala, H_2SO_4 formation from the gas-phase reaction of stabilized

648 Criegee Intermediates with SO_2 : Influence of water vapour content and temperature,

649 Atmos. Environ., 89, 603-612 (2014).

650

651 Berndt, T., T. Jokinen, R. L. Mauldin, III, T. Petäjä, H. Herrmann, H. Junninen, P.

652 Paasonen, D. R. Worsnop, and M. Sipilä, Gas-phase ozonolysis of selected olefins:

653 the yield of stabilized Criegee intermediates and the reactivity toward SO_2, *J. Phys.*

654 *Chem. Lett., 3*, 2892−2896 and supplement (2012).

655

656   Berresheim, H., J. McGrath, M. Adam, R.L. Mauldin III, B. Bohn, and F. Rohrer,

657   Seasonal Measurements of OH, NOx, and J(O^{1}D) at Mace Head, Ireland, *Geophys.*

658   *Res. Lett., 40,* 1659-1663 (2013).

659

660   Berresheim, H., T. Elste, H. G. Tremmel, A. G. Allen, H.-C. Hansson, K. Rosman, M.

661   DalMaso, J. M. Mäkelä, M. Kulmala, and C. D. O'Dowd, Gas-aerosol relationships of

662   H_2SO_4, MSA, and OH: Observations in the coastal marine boundary layer at Mace

663   Head, Ireland, *J. Geophys. Res.*, *107*(D19), 8100, doi: 10.1029/2000JD000229 (2002).

664

665   Berresheim, H., T. Elste, C. Plass-Dülmer, F.L. Eisele, and D.J. Tanner, Chemical

666   ionization mass spectrometer for long-term measurements of atmospheric OH and

667   H_2SO_4, *Int. J. Mass Spectrom.*, *202*, 91-109 (2000).

668

669   Berresheim, H., P. H. Wine, and D. D. Davis, Sulfur in the atmosphere, in

670   *Composition,Chemistry, and Climate of the Atmosphere*, edited by H. B. Singh, pp.

671   251-307, Van Nostrand Reinhold, New York (1995).

672

673   Berresheim, H., F. L. Eisele, and D. J. Tanner, Field studies of atmospheric DMS

674   chemistry using selected ion chemical ionization mass spectrometry, in

675   *Dimethylsulfide: Oceans, Atmosphere and Climate*, edited by G. Restelli, and G.

676   Angeletti, pp. 239-242, Kluwer Academic Publishers, Dordrecht (1993a).

677

678   Berresheim, H., F. L. Eisele, D. J. Tanner, D. S. Covert, L. McInnes, and D. C.

679   RamseyBell, Atmospheric sulfur chemistry and cloud condensation nuclei (CCN)

680   concentrations over the northeastern Pacific coast, *J. Geophys. Res.*, *98*, 12701-12711

681 (1993b).

682

683 Berresheim, H., and W. Jaeschke, Study of metal aerosol systems as a sink for

684 atmospheric SO_2, *J. Atmos. Chem.*, *4*, 311-334 (1986).

685

686 Bialek, J., M. Dall'Osto, C. Monahan, D. Beddows, and C. O'Dowd, On the

687 contribution of organics to the North East Atlantic aerosol number concentration,

688 *Environ. Res. Lett., 7*, doi:10.1088/1748-9326/7/4/044013 (2012).

689

690 Bohn, B., G. K. Corlett, M. Gillmann, S. Sanghavi, G. Stange, E. Tensing, M.

691 Vrekoussis, W. J. Bloss, L. J. Clapp, M. Kortner, H.-P. Dorn, P. S. Monks, U. Platt,

692 C. Plass-Dülmer, N. Mihalopoulos, D. E. Heard, K. C. Clemitshaw, F. X. Meixner, A.

693 S. H. Prevot, and R. Schmitt, Photolysis frequency measurement techniques: Results

694 of a comparison within the ACCENT project, *Atmos. Chem. Phys., 8*, 5373–5391

695 (2008).

696

697 Bossolasco, A., E. P. Faragó, C. Schoemaecker, C. Fittschen, Rate constant of the

698 reaction between CH_3O_2 and OH radicals, *Chem. Phys. Let., 593*, 7-13 (2014)

699

700 Boy, M., D. Mogensen, S. Smolander, L. Zhou, T. Nieminen, P. Paasonen, C. Plass-

701 Dülmer, M. Sipilä, T. Petäjä, L. Mauldin, H. Berresheim, and M. Kulmala, Oxidation

702 of SO_2 by stabilized Criegee intermediate (sCI) radicals as a crucial source for

703 atmospheric sulfuric acid concentrations, *Atmos. Chem. Phys., 13*, 3865-3879 (2013).

704

705 Boy, M., M. Kulmala, T. Ruuskanen, M. Pihlatie, A. Reissell, P. P. Aalto, P. Keronen,

706 M. Dal Maso, H. Hellen, H. Hakola, R. Janssen, M. Hanke, and F. Arnold, Sulphuric

707 acid closure and contribution to nucleation mode particle growth, *Atmos. Chem.*

708 *Phys., 5,* 863–878 (2005).

709

710 Broadgate, W.J., G. Malin, F.C. Küpper, A. Thompson, and P.S. Liss, Isoprene and

711 other non-methane hydrocarbons from seaweeds: a source of reactive hydrocarbons to

712 the atmosphere, *Marine Chem., 88*, 61– 73 (2004).

713

714 Calvert, J. G., R. Atkinson, J.A. Kerr, S. Madronich, G.K. Moortgat, T.J. Wallington,

715 and G. Yarwood, *The mechanisms of atmospheric oxidation of alkenes*, Oxford

716 University Press, New York, ISBN 0-19-513177-0 (2000).

717

718 Commane, R, K. Seitz, C. S. E. Bale, W. J. Bloss, J. Buxmann, T. Ingham, U. Platt,

719 D. Pöhler, and D. E. Heard, Iodine monoxide at a clean marine coastal site:

720 observations of high frequency variations and inhomogeneous distributions, *Atmos.*

721 *Chem. Phys., 11,* 6721-6733 (2011).

722

723 Cox, R.A., and S.A. Penkett, Oxidation of atmospheric SO_2 by products of the ozone–

724 olefin reaction, *Nature, 230,* 321-322 (1971).

725

726 Criegee, R., Mechanism of ozonolysis, Angew. Chem.-Int. Edit. Engl.,14, 745-752

727 (1975).

728

729   Davis, D. G. Chen, P. Kasibhatla, A . Jefferson, D . Tanner, F. Eisele, D. Lenschow,

730   W . Neff, and H . Berresheim, DMS oxidation in the Antarctic marine boundary

731   layer: Comparison of model simulations and field observations of DMS, DMSO,

732    $DMSO_2$, $H_2SO_4(g)$, MSA(g), and MSA(p), *J. Geophys. Res., 103,* 1657-1678 (1998).

733

734   De Bruyn, W. J., J. A. Shorter, P. Davidovits, D. R. Worsnop, M. S. Zahniser, and C.

735   E. Kolb, Uptake of gas phase sulfur species methanesulfonic acid, dimethylsulfoxide,

736   and dimethyl sulfone by aqueous surfaces, *J. Geophys. Res., 99(D8),* 16927–16932,

737   doi:10.1029/94JD00684 (1994).

738

739   DeMore, W.B., S.P. Sander, D.M. Golden, R.F. Hampson, M.J. Kurylo, C.J. Howard,

740   A.R. Ravishankara, C.E. Kolb, and M.J. Molina, Chemical kinetics and

741   photochemical data for use in stratospheric modeling. Evaluation number *12*, JPL

742   Publication *97-4*, 1 – 266 (1997).

743

744   Eisele, F. and D. Tanner, Measurement of the gas phase concentration of H_2SO_4 and

745   methane sulfonic acid and estimates of H_2SO_4 production and loss in the atmosphere,

746   *J. Geophys. Res,. 98,* 9001–9010 (1993).

747

748   Eisele, F. L.*,* and D. J. Tanner*,* Ion-assisted tropospheric OH measurements*, J.*

749   *Geophys. Res., 96(D5),* 9295–9308*,* (1991).

750

751   Fittschen, C., L. K. Whalley, and D. E. Heard, The reaction of CH_3O_2 radicals with

752   OH radicals: a neglected sink for CH_3O_2 in the remote atmosphere, *Environmental*

753   *Science & Technology, 48 (14)*, 7700-7701 (2014)

754

755 Foresman, J.B., and A. Frisch, *Exploring chemistry with electronic structure methods*.

756 Gaussian, Inc., Pittsburgh (1996).

757

758 Frisch, M.J., G. W. Trucks, H. B. Schlegel, G. E. Scuseria, M. A. Robb, J. R.

759 Cheeseman, G. Scalmani, V. Barone, B. Mennucci, G. A. Petersson, H. Nakatsuji, M.

760 Caricato, X. Li, H. P. Hratchian, A. F. Izmaylov, J. Bloino, G. Zheng, J. L.

761 Sonnenberg, M. Hada, M. Ehara, K. Toyota, R. Fukuda, J. Hasegawa, M. Ishida, T.

762 Nakajima, Y. Honda, O. Kitao, H. Nakai, T. Vreven, J. A. Montgomery, Jr., J. E.

763 Peralta, F. Ogliaro, M. Bearpark, J. J. Heyd, E. Brothers, K. N. Kudin, V. N.

764 Staroverov, R. Kobayashi, J. Normand, K. Raghavachari, A. Rendell, J. C. Burant, S.

765 S. Iyengar, J. Tomasi, M. Cossi, N. Rega, J. M. Millam, M. Klene, J. E. Knox, J. B.

766 Cross, V. Bakken, C. Adamo, J. Jaramillo, R. Gomperts, R. E. Stratmann, O. Yazyev,

767 A. J. Austin, R. Cammi, C. Pomelli, J. W. Ochterski, R. L. Martin, K. Morokuma, V.

768 G. Zakrzewski, G. A. Voth, P. Salvador, J. J. Dannenberg, S. Dapprich, A. D. Daniels,

769 Ö. Farkas, J. B. Foresman, J. V. Ortiz, J. Cioslowski, and D. J. Fox, Gaussian 09,

770 Revision A.1. Gaussian, Inc. (2009).

771

772 Fuchs, N., and A. Sutugin, Highly dispersed aerosol, in *Topics in Current Aerosol*

773 *Research*, edited by G. Hidy and J. Brock, Pergamon, New York (1971).

774

775 Glukhovtsev, M. N., A. Pross, M.P. McGrath, and L. Radom, Extension of Gaussian-

776 2 (G2) theory to bromine- and iodine-containing molecules: Use of effective core

777 potentials, *J. Chem. Phys.*, *103*, 1878-1885 (1995).

778

779   Hanson, D.R., Mass accommodation of H_2SO_4 and CH_3SO_3H on water-sulfuric acid

780   solutions from 6% to 97% rH, *J. Phys. Chem. A, 109*, 6919-6927 (2005).

781

782   Harris, E., B. Sinha, D. van Pinxteren, A. Tilgner, K. W. Fomba, J. Schneider, A.

783   Roth, T. Gnauk, B. Fahlbusch, S. Mertes, T. Lee, J. Collett, S. Foley, S. Borrmann, P.

784   Hoppe, and H. Herrmann, Enhanced role of transition metal ion catalysis during in-

785   cloud oxidation of SO_2, *Science, 340*, 727-730 (2013).

786

787   Heard, D.E., and M.J. Pilling, Measurement of OH and HO_2 in the troposphere,

788   *Chem. Rev., 103,* 5163-5198 (2003).

789

790   Huey, G.L., Measurement of trace atmospheric species by chemical ionization mass

791   spectrometry: Speciation of reactive nitrogen and future directions, *Mass Spectrom.*

792   *Rev., 26*, 166-184 (2007)

793

794   Jefferson, A., D. J. Tanner, F. L. Eisele, and H. Berresheim, Sources and sinks of

795   H_2SO_4 in the remote Antarctic marine boundary layer, *J. Geophys. Res.*, *103*, 1639-

796   1645 (1998).

797

798   Jenkin, M. E., Saunders, S. M., Wagner, V., and Pilling, M. J.: Protocol for the

799   development of the Master Chemical Mechanism, MCM v3 (Part B): tropospheric

800   degradation of aromatic volatile organic compounds, *Atmos. Chem. Phys., 3*, 181–193

801   (2003)

802

803 Kolb, C.E., R. A. Cox, J. P. D. Abbatt, M. Ammann, E. J. Davis, D. J. Donaldson, B.

804 C. Garrett, C. George, P.T. Griffiths, D. R. Hanson, M. Kulmala, G. McFiggans, U.

805 Pöschl, I. Riipinen, M. J. Rossi, Y. Rudich, P. E. Wagner, P. M. Winkler, D. R.

806 Worsnop, and C. D. O' Dowd, An overview of current issues in the uptake of

807 atmospheric trace gases by aerosols and clouds, *Atmos. Chem. Phys., 10,* 10561–

808 10605 (2010).

809

810 Kreidenweis, S. M., and J. H. Seinfeld, Nucleation of sulfuric acid water and

811 methanesulfonic acid-water solution particles: Implications for the atmospheric

812 chemistry of organosulfur species, *Atmos. Environ., 22,* 283–296 (1988).

813

814 Kroll, J. H., R.S. Shailesh, J.G. Anderson, K.L. Demerjian, and N.M. Donahue,

815 Mechanism of HOx formation in the gas-phase ozone-alkene reaction. 2. Prompt

816 versus thermal dissociation of carbonyl oxides to form OH, *J. Phys. Chem. A, 105,*

817 4446−4457 (2001).

818

819 Krouse, H.R., and V.A. Grinenko (Eds.), *Stable Isotopes: Natural and Anthropogenic*

820 *Sulphur in the Environment*, Scientific Committee on Problems of the Environment

821 (SCOPE), vol. 43, J. Wiley & Sons, Chichester (1991).

822

823 Larin, I.K., N. A. Messineva, A. I. Spasskii, E. M. Trofimova, and L. E. Turkin,

824 Measurement of the rate constants for the reactions of the $IO^{\bullet}$ radical with sulfur-

825 containing compounds H_2S, $(CH_3)_2S$, and $SO_2,$ *J. Kinetics and Catalysis, 41,* 437-443

826 (2000).

827

828   Lewis, A.C., J.B. McQuaid, N. Carslaw, and M.J. Pilling, Diurnal cycles of short-

829   lived tropospheric alkenes at a north Atlantic coastal site, *Atmos. Environ., 33*, 2417-

830   2422 (1999).

831

832   Lin, C.T., A.R. Baker, T.D. Jickells, S. Kelly, and T. Lesworth, An assessment of the

833   significance of sulphate sources over the Atlantic Ocean based on sulphur isotope

834   data, *Atmos. Environ., 62*, 615-621 (2012).

835

836   Lin, X., and W.L. Chameides, CCN formation from DMS oxidation without SO_2

837   acting as an intermediate, *Geophys. Res. Lett., 20,* 579-582 (1993).

838

839   Liu, Y., K.D. Bayes, and S.P. Sander, Measuring rate constants for reactions of the

840   simplest Criegee intermediate (CH_2OO) by monitoring the OH radical, *J. Phys. Chem.*

841   *A, 118*, 741-747 (2014).

842

843   Mauldin III, R.L., T. Berndt, M. Sipilä, P. Paasonen, T. Petäjä, S. Kim, T. Kurtén, F.

844   Stratmann, V.-M. Kerminen, and M. Kulmala, A new atmospherically relevant

845   oxidant of sulphur dioxide, *Nature, 488,* 193-196 and supplement, (2012).

846

847   Mauldin, R., III, G. Frost, G. Chen, D. Tanner, A. Prevot, D. Davis, and F. Eisele, OH

848   measurements during the First Aerosol Characterization Experiment (ACE 1):

849   Observations and model comparisons, *J. Geophys. Res., 103*, 16713–16729 (1998).

850

851   Montgomery Jr., J.A., M. J. Frisch, J. W. Ochterski, and G. A. Petersson, A complete

852   basis set model chemistry. VII. Use of the minimum population localization method,

853   *J. Chem. Phys.*, *112*, 6532-6542 (2000).

854

855   O'Dowd, C.D., J.L. Jimenez, R. Bahreini, R.C. Flagan J.H. Seinfeld, K. Hämeri, L.

856   Pirjola, M. Kulmala, S.G. Jennings, and T. Hoffmann, Marine particle formation from

857   biogenic iodine emissions, *Nature, 417*, 632-636 (2002).

858

859   Ovadnevaite, J., D. Ceburnis, S. Leinert, M. Dall'Osto, M. Canagaratna, P. O'Brien,

860   S. O'Doherty, H. Berresheim, and C. O'Dowd, Distinct seasonal changes in marine

861   aerosol composition and its properties, *J. Geophys. Res.,* submitted (2014).

862

863   Seinfeld, J.H., and S.N. Pandis, *Atmospheric Chemistry and Physics – From Air*

864   *Pollution to Climate Change*, chapters 8 and 11, J. Wiley & Sons, New York (1998).

865

866   Saiz-Lopez, A., J. A. Shillito, H. Coe, and J. M. C. Plane, Measurements and

867   modelling of I_2, IO, OIO, BrO and NO_3 in the mid-latitude marine boundary layer,

868   *Atmos. Chem. Phys., 6*, 1513–1528 (2006).

869

870   Saiz-Lopez, A., and J.M.C. Plane, Novel iodine chemistry in the marine boundary

871   layer, *Geophys. Res. Lett.*, *31*, doi: L04112 (2004).

872

873   Saiz-Lopez, A., J.M.C. Plane, and J.A. Shillito, Bromine oxide in the mid-latitude

874   marine boundary layer, *Geophys. Res. Lett.*, *31*, doi: L03111 (2004).

875

876 Sarwar, G., H. Simon, K. Fahey, R. Mathur, W.S. Goliff, and W.R. Stockwell, Impact

877 of sulfur dioxide oxidation by Stabilized Criegee Intermediate on sulfate, Atmos.

878 Environ., 85, 204-214 (2014).

879

880 Saunders, S. M., Jenkin, M. E., Derwent, R. G., and Pilling, M.J.: Protocol for the

881 development of the Master Chemical Mechanism, MCM v3 (Part A): tropospheric

882 degradation of nonaromatic volatile organic compounds, *Atmos. Chem. Phys., 3*, 161–

883 180, (2003).

884

885 Seguin, A.M., A.-L. Norman, S. Eaton, M. Wadleigh, and S. Sharma, Elevated

886 biogenic sulphur dioxide concentrations over the North Atlantic, *Atmos. Environ., 44*,

887 1139-1144 (2010).

888

889 Schweitzer, F., L. Magi, P. Mirabel, and C. George, Uptake rate measurements of

890 methanesulfonic acid and glyoxal by aqueous droplets, *J. Phys. Chem. A, 102*, 593–

891 600 (1998).

892

893 Stone, D., M. Blitz, L. Daubney, N.U.M. Howes, and P. Seakins, Kinetics of CH_2OO

894 reactions with SO_2, NO_2, NO, H_2O and CH_3CHO as a function of pressure, *Phys.*

895 *Chem. Chem. Phys., 16*, 1139-1149 (2014).

896

897 Stone, D., M. Blitz, L. Daubney, T. Ingham, and P. Seakins, CH_2OO Criegee biradical

898 yields following photolysis of CH_2I_2 in O_2, *Phys. Chem. Chem. Phys., 15*, 19119-

899 19124 (2013).

900

901   Stone, D., L.K. Whalley, and D.E. Heard, Tropospheric OH and HO_2 radicals: field

902   measurements and model comparisons, *Chem. Soc. Rev., 41,* 6348-6404 (2012).

903

904   Taatjes, C.A., D.E. Shallcross, and C. J. Percival, Research frontiers in the chemistry

905   of Criegee intermediates and tropospheric ozonolysis, *Phys. Chem. Chem. Phys.,*

906   16(5), 1704-1718 (2014).

907

908   Taatjes, C.A., Welz, O., Eskola, A.J., Savee, J.D., Scheer, A.M., Shallcross, D.E.,

909   Rotavera, B., Lee, E.P.F., Dyke, J.M., Mok, D.K.W., Osborn, D.L., and C.J. Percival,

910   Direct measurements of conformer-dependent reactivity of the Criegee intermediate

911   CH_3CHOO, *Science, 340*, 177-180, DOI: 10.1126/science.1234689 (2013)

912

913   Tanner, D. J.*,* and F. L. Eisele, Present OH measurement limits and associated

914   uncertainties*, J. Geophys. Res., 100(D2),* 2883–2892 (1995).

915

916   Vereecken, L., H. Harder, and A. Novelli, The reaction of Criegee intermediates with

917   NO, RO_2, and SO_2, and their fate in the atmosphere, *Phys. Chem. Chem. Phys., 14*,

918   14682–14695 (2012).

919

920   Welz, O., J.D. Savee, D.L. Osborn, S.S. Vasu, C. Percival, D. E. Shallcross, C.A.

921   Taatjes, Direct kinetic measurements of Criegee intermediate (CH_2OO) formed by

922   reaction of CH_2I with O_2, *Science, 335,* 204-207 (2012).

923

924

925 **Figure Captions**

926

927 Figure 1. Principle scheme of SI/CIMS components including air inlet (modified from

928 R.L. Mauldin III, *pers. commun.,* 2012). Inset shows details of the atmospheric

929 pressure region with reagent gas flows indicated for measurement of OH background

930 signal (both $^{34}SO_2$ and C_3H_8 are added to the sample air through the two front

931 injectors; see text). Laminar flow conditions with a central flow axis velocity of 0.71

932 m s^{-1} in both the sample and ionization tubes are generated by a 12 slpm sample flow,

933 58 slpm total flow (= sample flow plus sheath flow, the latter indicated here by

934 addition of *Air/HNO₃ mixture*), and the geometries of the sample tube (diameter 1.9

935 cm) and ionization tube (diameter 4.2 cm). The time needed (in each case starting at

936 the first injector) to reach the second injector is 73 ms, to the entrance of the

937 ionization region 115 ms, and to the aperture in front of the mass spectrometer 450

938 ms, respectively.

939

940 Figure 2. Midday (1000-1400 UTC) maximum H_2SO_4 and MSA(g) concentrations in

941 marine air at Mace Head, averaged for each month (total measurement period: May

942 2010 – August 2012). Vertical bars denote standard deviations.

943

944 Figure 3. Correlation between H_2SO_4 and OH (top) and between MSA(g) and OH

945 concentrations (bottom) in marine air for the period May - August 2011 (5 min

946 integrated data, daytime: 0800-2000 UTC). To match the measured data in time OH

947 concentrations were calculated based on concurrent $J(O^1D)$ data and the $J(O^1D)$-OH

948 relationship for marine air previously established in Berresheim et al. [2013].

949

950 Figure 4. (top) SO_2 mixing ratios (1 hour signal integration) measured in marine air

951 between May – August 2011 (average: 160 ($\pm$ 50) pptv; detection limit: 25 pptv,

952 indicated by red line); (bottom) Condensational sink (CS; 5 min integration)

953 calculated for H_2SO_4 (see text).

954

955 Figure 5a. Example of observed ambient H_2SO_4 concentration in comparison with

956 H_2SO_4 mass balance values calculated from eq. (1) for 18 June 2011. Air masses

957 originated from polar regions between Greenland and Iceland exhibiting strong

958 biological activity in surface waters. As OH had only been measured for 5 min during

959 each half hour period, to obtain calculated H_2SO_4 for each of the corresponding

960 measured H_2SO_4 values we used $J(O^1D)$ as proxy for OH to fill the corresponding gaps

961 based on the OH-$J(O^1D)$ relation established for the marine sector [Berresheim et al.,

962 2013] (continuous 5 min time resolution). (top) Mean discrepancy factor of 7.0

963 between midday (1000-1400 UTC) observed and calculated $[H_2SO_4]$. Open symbols

964 show calculated $[H_2SO_4]$ based on actual OH measurement signals (ratio: 5.6$\pm$1.2).

965 (bottom) Signal counts obtained for OH measurement (OH plus background) and

966 background mode only (cycle: 5 min during each 30 min period).

967

968 Figure 5b. Example of relatively small discrepancy between measured and calculated

969 H_2SO_4 based on eq (1) (ratio 1.8) and actual OH measurements (ratio 2.5$\pm$1.2),

970 respectively. Nighttime OH values were with one exception below the detection limit.

971 For further explanations see Figure 5a caption and text. Air mass origin was mainly

972 from temperate North Atlantic in connection with anticyclonic conditions.

973

974   Figure 6. Mean half-hour values measured in marine air during the time period 2010-

975   2011 calculated from the OH mode raw signal at m/z 99 (blue line), total background

976   mode raw signal at m/z 99 (red line), OH mode signal minus background mode signal

977   (green line = net signal counts corresponding to the ambient OH concentration),

978   signal counts at m/z 99 due to ^{34}S mass fraction of ambient H_2SO_4 (black dashed line

979   = signal(m/z 97)*0.044), OH mode background signal with ^{34}S fraction of ambient

980   H_2SO_4 subtracted (red dashed line).

981

982   Figure 7. Transition state geometries for ClO, BrO, IO and OIO + SO_2.

983

984   Figure 8a. Example observation showing relationships between aerosol nucleation

985   events at low tide, OH concentrations, and OH background (BG) signal (due to X-

986   compound). (top) H_2SO_4 and MSA(g) concentrations (30 s integration), tidal height,

987   and total particle number concentration $N_p > 3$ nm diameter (30 s integration)

988   measured with a condensation particle counter (CPC; TSI 3025). (bottom) OH

989   concentrations (5 min; black dots), count rates for OH+BG and BG only (non-OH)

990   signals (30 s), and ozone photolysis frequency, $J(O^1D)$.

991

992   Figure 8b. Example of increased OH concentrations and OH background signal (BG)

993   during two aerosol nucleation events at low tide under marine sector conditions.

994   Symbols as in Figure 8a.

995

996
997
998
999   Table 1. Molecular parameters and energies for transition state theory calculations (see text

1000   for theoretical methods). The symbol [#] indicates a transition state.

Species	Transition state geometry[a]	Rotational constants / GHz	Vibrational frequencies / cm^{-1}	Relative energy[b] / kJ mol^{-1}
ClO		18.03	829	-
SO$_2$		58.67, 10.17, 8.667	508, 1146, 1334	-
ClO-SO$_2$[#]	Cl: 2.906, 0.862, -0.283 O: 1.988, -0.503, -0.103 S: -0.021, -0.255, -0.325 O: -0.353, 1.084, 0.116 O: -0.553, -1.414, 0.357	8.227, 1.831, 1.540	248i, 73, 135, 270, 296, 492, 720, 1113, 1303	24.1
BrO		12.50	713	-
BrO-SO$_2$[#]	Br: -0.048, 0.360, 0.367 O: 0.235, -0.502, 1.910 S: 1.906, 0.0189, 3.011 O: 2.914, 0.483, 2.075 O: 2.140, -1.167, 3.803	8.138, 1.128, 1.011	239i, 63, 114, 227, 280, 494, 625, 1115, 1302	20.4
IO		9.844	649	-
IO-SO$_2$[#]	I: 1.387, 0.0252, 0.0250 O: -0.292, -0.940, -0.130 S: -2.056, 0.068, 0.307 O: -1.803, 1.417, 0.167 O: -2.984, -0.780, 0.412	8.050, 0.875, 0.806	258i, 73, 109, 222, 292, 495, 613, 1107, 1288	7.3
OIO		18.31, 7.054, 5.092	273, 809, 831	-
OIO-SO$_2$[#]	S: -0.005, 0.236, 0.0738 O: 0.210, 0.766, 1.416 O: 1.111, -0.069, -0.803 I: -1.644, 3.069, 0.096 O: -0.961, 1.427, -0.805 O: -0.190, 4.124, 0.404	4.572, 0.871, 0.839	304i, 29, 79, 129, 202, 261, 417, 495, 547, 810, 1064, 1247	50.1

1001

1002   [a] Atomic positions in Cartesian coordinates (Å)

1003   [b] above the reactants, including zero-point energies

1004

1005

1006

43

1007 **Table 2: Details of the calculation of the relative oxidation efficiency (ROE, see**
1008 **Eq.(5)) for specific Criegee intermediates assuming ozonolysis of alkenes as their**
1009 **only source of formation for average ambient conditions at Mace Head (14°C,**
1010 **75% RH, $BG_{sig}/OH_{sig}=1$)**

1011

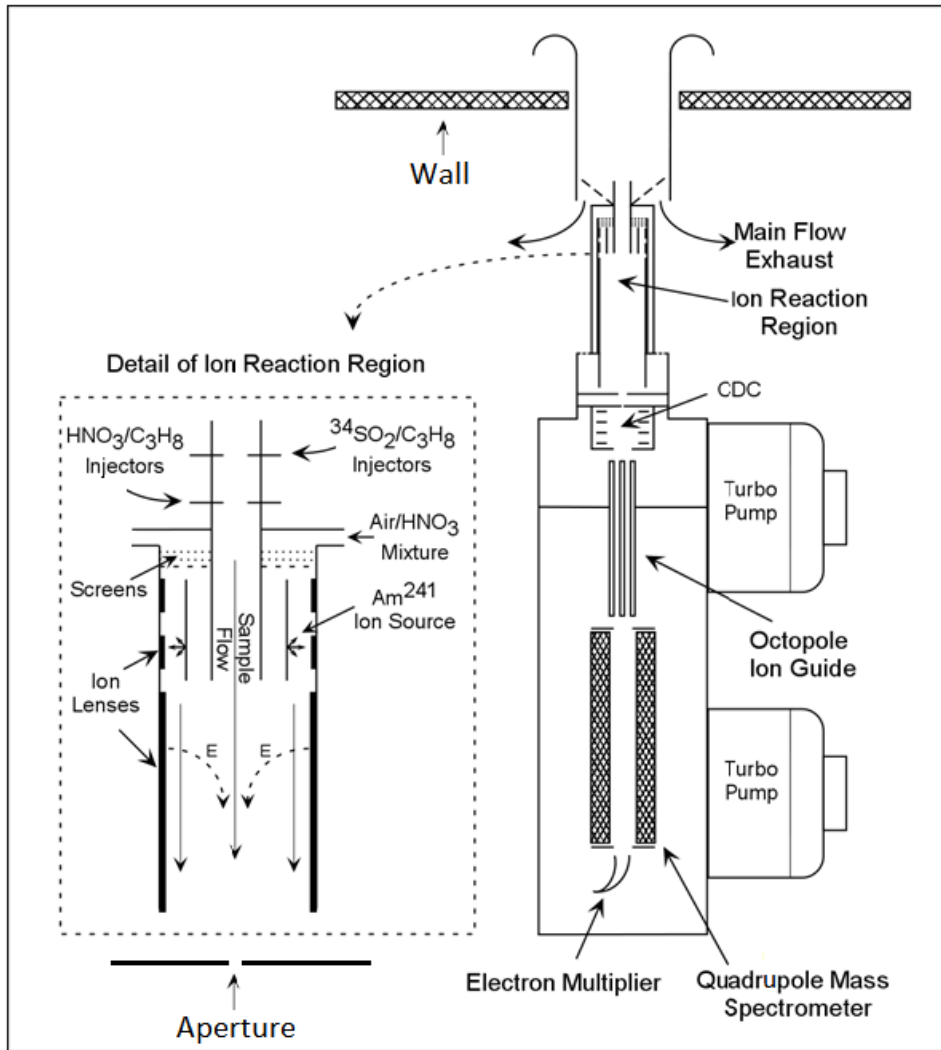|	CH_2OO	*anti-* CH_3CHOO	*syni-* CH_3CHOO	α-pinene	limonene
$k(sCI+SO_2)$ [cm^3 s^{-1}]	$3.9\times10^{-11\,a}$	$6.7\times10^{-11\,b}$	$2.4\times10^{-11\,b}$	5.9×10^{-13c}	$7.7\times10^{-13\,c}$
$k(sCI+H_2O)$ [cm^3 s^{-1}]	$<9\times10^{-17\,d}$	$1\times10^{-14\,b}$	$<4\times10^{-15\,b}$	1.4×10^{-17} e	$1.4\times10^{-17\,e}$
τ^{-1}(unimolecular) [s^{-1}]	$500^{\,a}$ $<100^{\,f}$	$<250^{\,b}$	$<250^{\,b}$	$5^{\,c}$	$5^{\,c}$
τ^{-1}(8ppm SO_2) [s^{-1}]	7800	13400	4800	118	154
τ^{-1}(ambient H_2O) [s^{-1}]	$27^{\,d}$ $(2840)^{\,f}$	3000	1200	4.2	4.2
EF (Eq. 3)	150	919	411	3.6	3.6
$k(sCI+SO_2)$ / $k(OH+SO_2)$	43.3	74.4	26.7	0.66	0.86
ROE (Eq.5)	0.29 $(0.05)^{\,f}$	$0.09\text{-}0.08^{\,g}$	$0.08\text{-}0.06^{\,g}$	0.18	0.24
Fraction of sCI reacting with $^{34}SO_2$ in the CIMS inlet	0.94	0.80	0.77	0.93	0.94

1012 a: Welz et al. [2012]   b: Taatjes et al. [2013]   c: Mauldin et al. [2012]

1013 d: Stone at al. [2014]   e: MCM 3.2   f: Berndt et al. [2014]

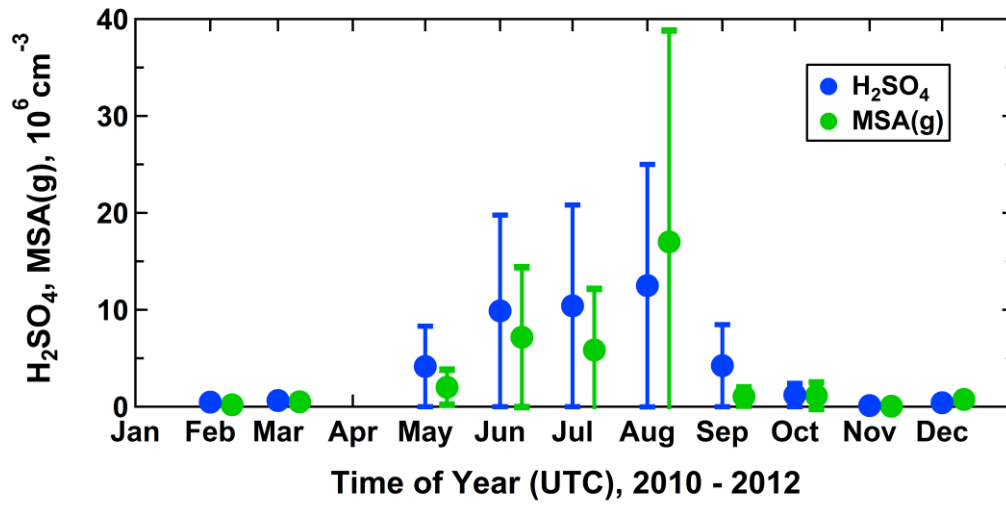1014 g: range reflecting unimolecular decomposition rates 0-250 s^{-1}

1015
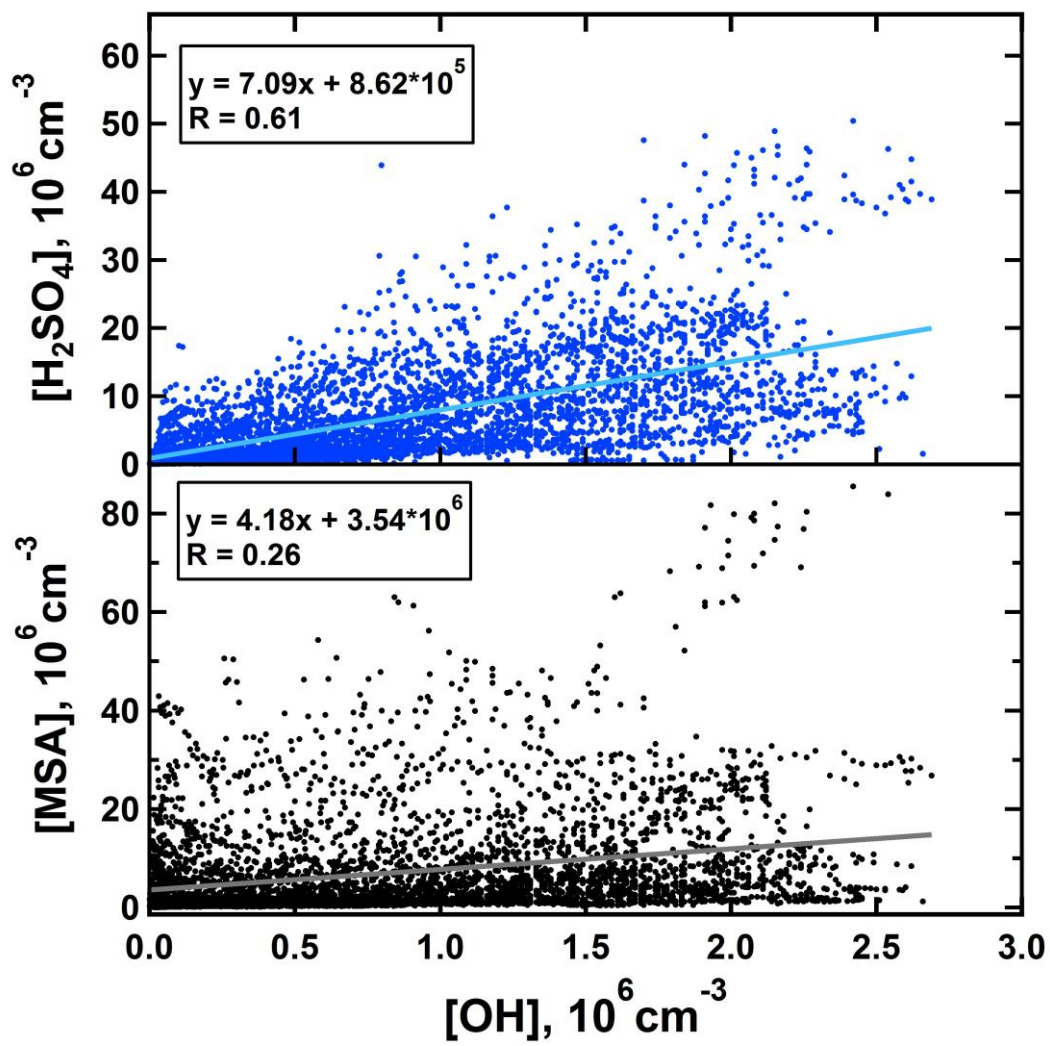
1016

1017

1018

1019   Figure 1

1020

1021

1022

1023   Figure 2.

1024

1025

The scatter plot shows two panels. The top panel plots $[H_2SO_4]$, 10^6 cm^{-3} versus $[OH]$, 10^6 cm^{-3} with the equation $y = 7.09x + 8.62 \times 10^5$ and $R = 0.61$. The bottom panel plots $[MSA]$, 10^6 cm^{-3} versus $[OH]$, 10^6 cm^{-3} with the equation $y = 4.18x + 3.54 \times 10^6$ and $R = 0.26$.
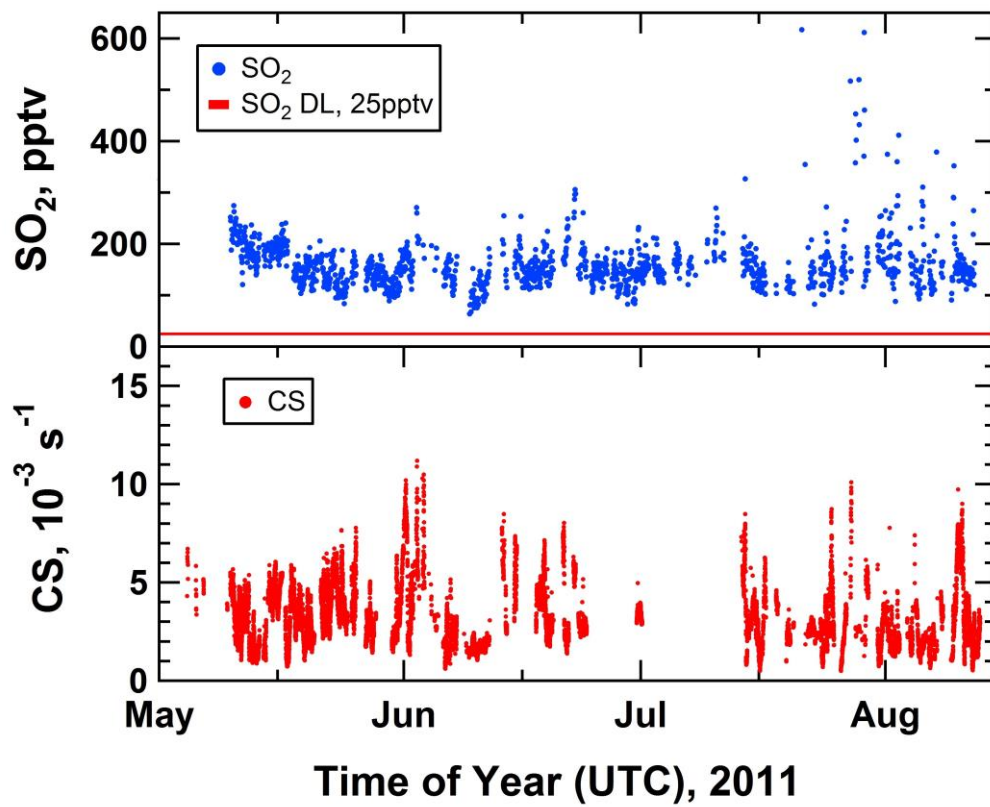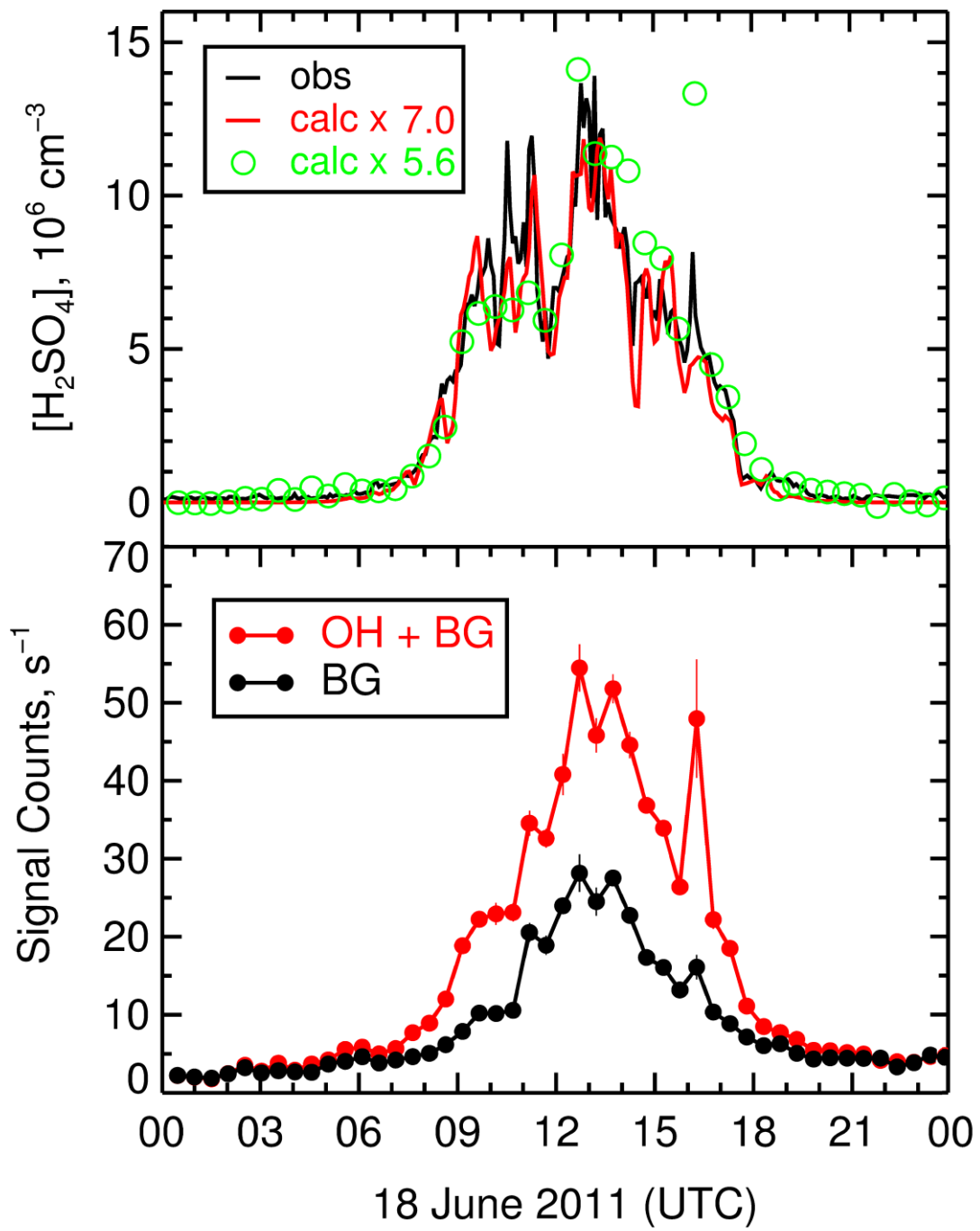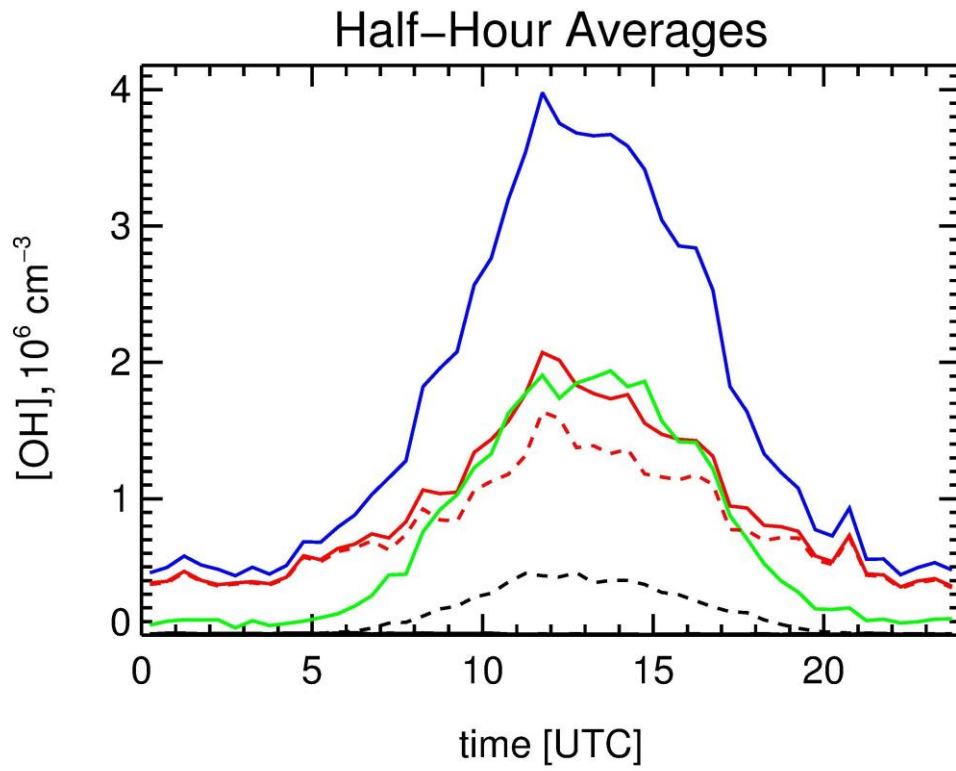
1026

1027

1028 Figure 3.

1029

1030

1031   Figure 4.

1032

1033

1034   Figure 5a.

1035

1036

1037   Figure 5b.

Half−Hour Averages

[OH], 10^6 cm^{-3} vs time [UTC]
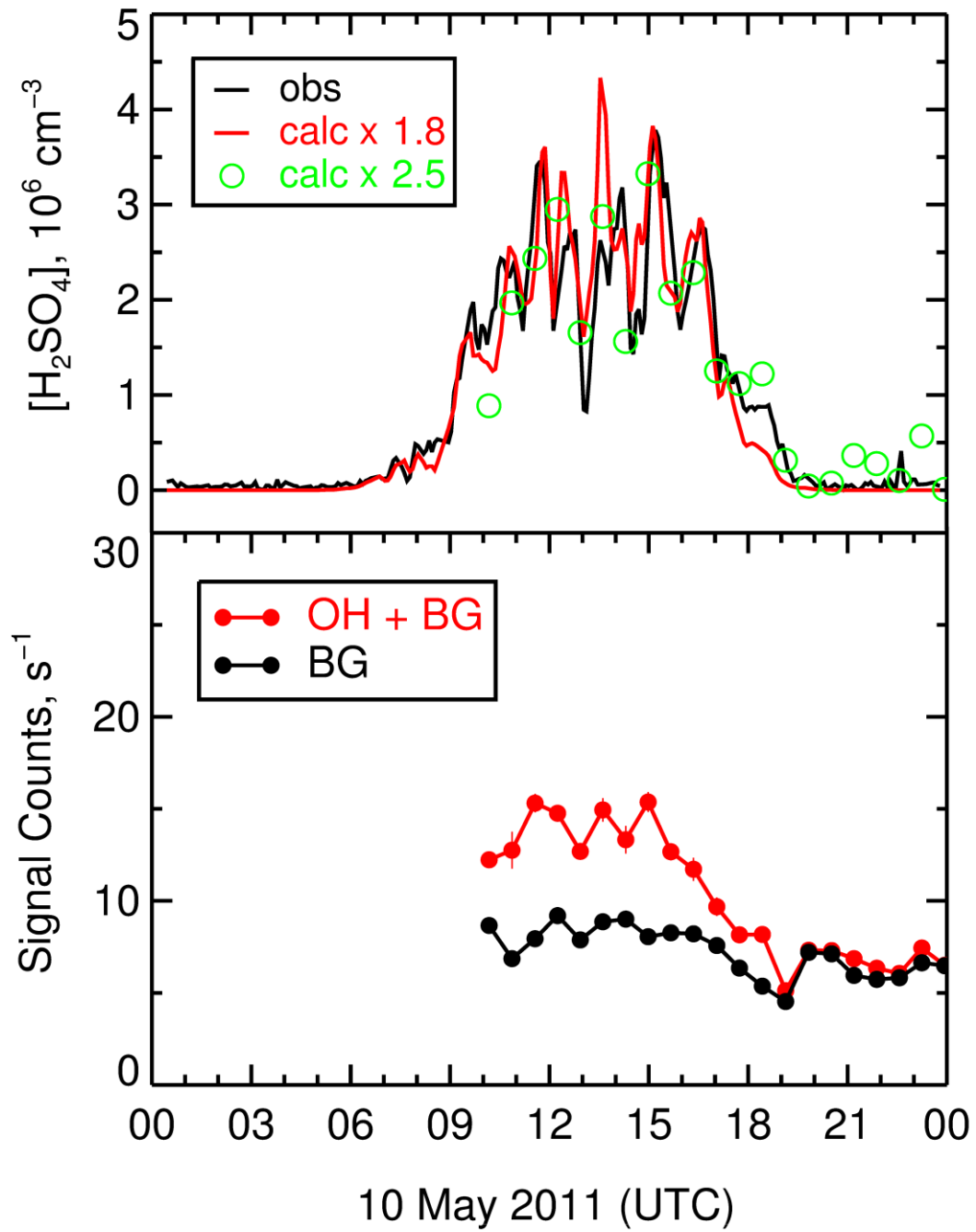
1038

1039   Figure 6.

1040

1041

3 Å
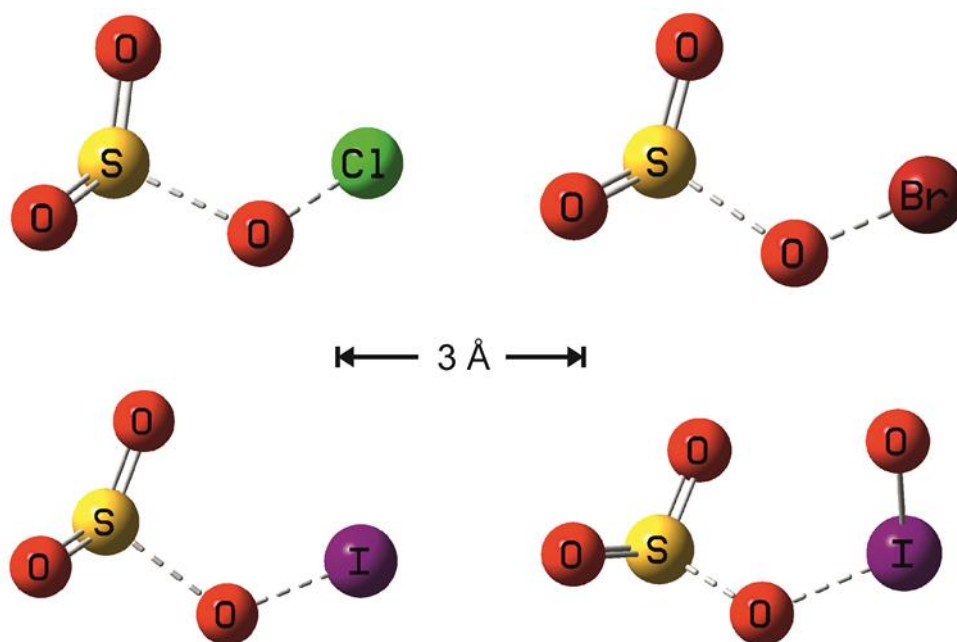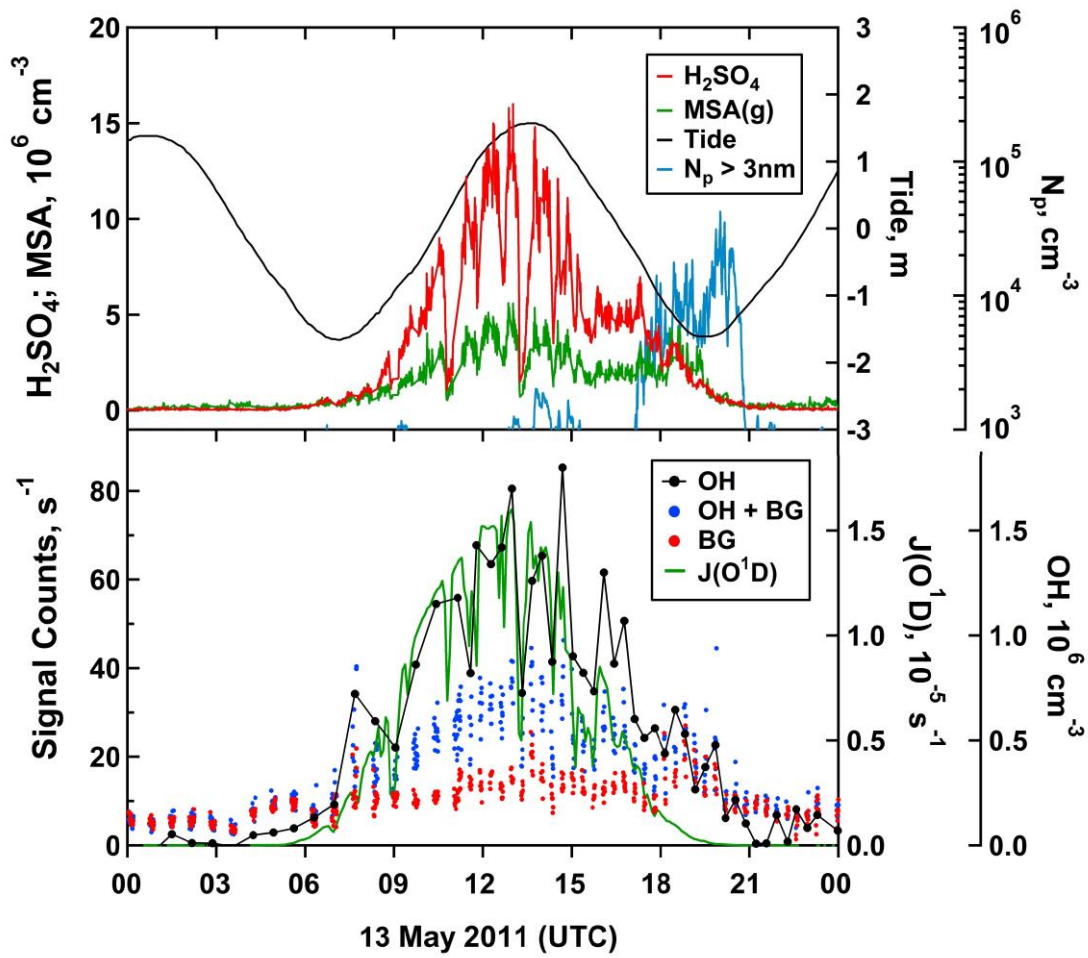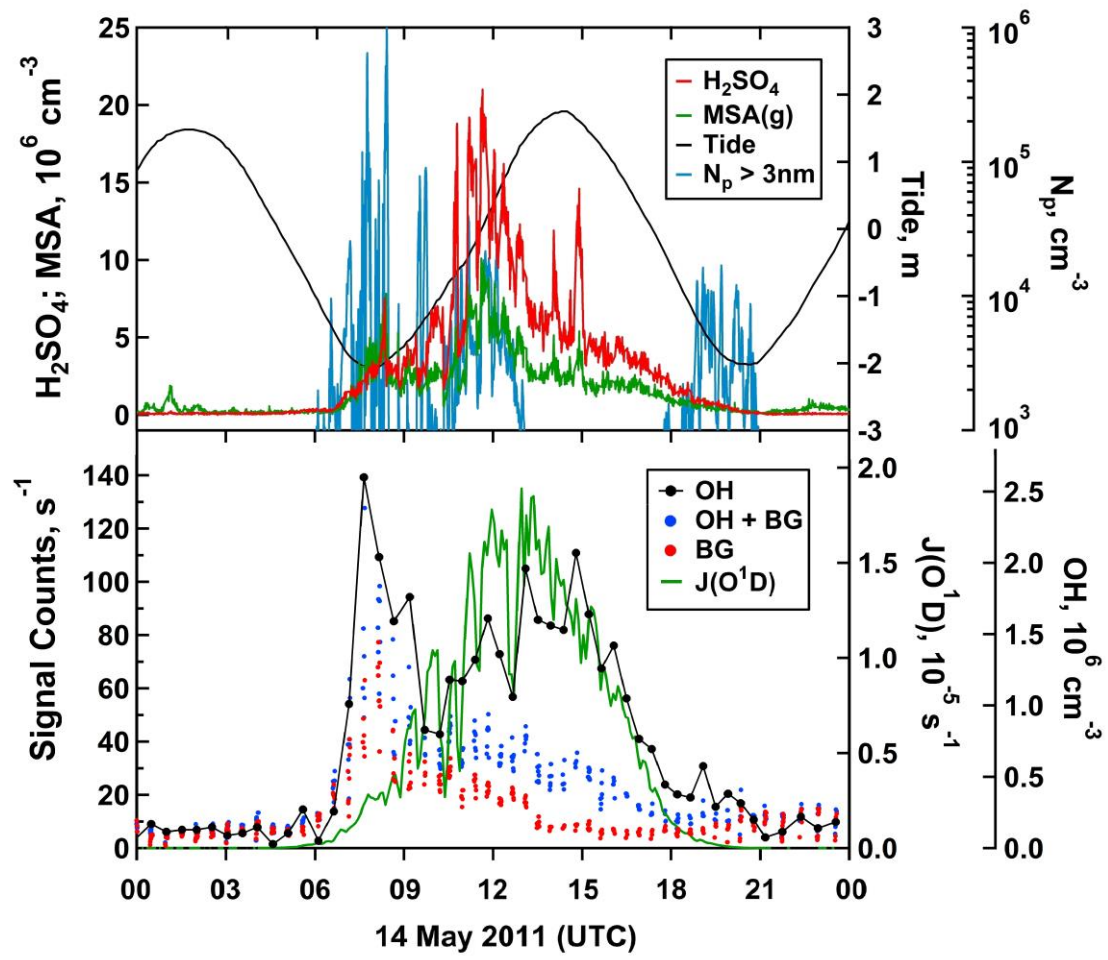
1042

1043

1044   Figure 7.

1045

1046

1047   Figure 8a.

1048

1049
1050   Figure 8b.